Improved Constitutive Model for Mesoscale Modelling of Unidirectional Composites

Master Thesis

Siddhesh G. Rajadhyaksha

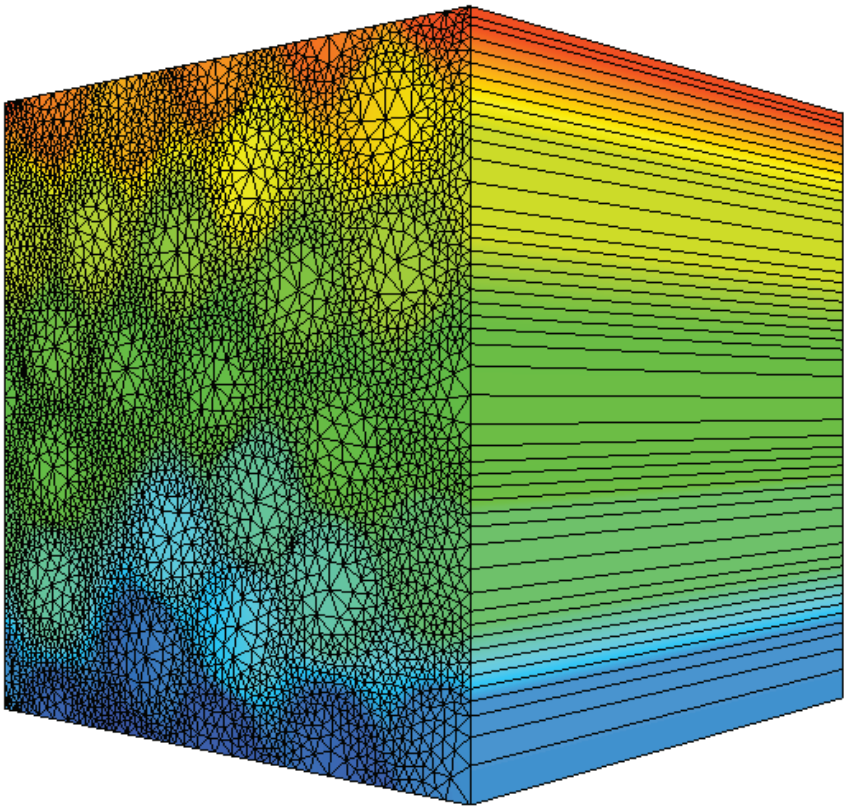

TU Delft Delft University of Technology

Improved Constitutive Model for Mesoscale Modelling of Unidirectional Composites

by

Siddhesh G. Rajadhyaksha

to obtain the degree of Master of Science
at the Delft University of Technology,
to be defended publicly on Monday November 30, 2020 at 02:00 PM.

Student number:	4820878	
Project duration:	March 1, 2020 – November 30, 2020	
Thesis committee:	Dr. ir. F.P. Van Der Meer,	TU Delft, Chair
	Debashis Wadadar MSc,	TU Delft, Supervisor
	Dr. Marco Pavlovic	TU Delft

TU Delft

Preface

This graduation project was undertaken to complete my master study in structural engineering with structural mechanics specialisation at the Delft University of Technology. Computational mechanics research group strives to quantify the various mechanical behaviours and processes in different types of materials, like composites, using computational tools. This thesis stems from a similar interest for better understanding and predicting of composite material behaviour. Thus, this research investigates methods to analyse the behaviour of unidirectional composites under the action of combined stresses. The focus is on estimating the nonlinear plastic behaviour of homogenized mesomodel with the help of micro models.

Although an individual project, it would not have been possible without the support of many people. I am thankful to my graduation committee for being very supportive and guiding me through the entire process. They gave me a lot of freedom to work, which was a great learning experience and helped me evolve in many ways, other than just academia.

I'd like to take this opportunity to especially thank my chair Dr. ir. F.P. Van Der Meer, who gave me the opportunity to work with the computational mechanics group in the Department of Civil Engineering and Geo sciences. He was prompt in his response when I was struggling with my work and kindly helped me out with setting up the code. I am truly grateful for his active guidance throughout my project.

I am grateful to my supervisor Debashis Wadadar who was ready for brainstorming sessions regarding my work. He provided valuable sources for me to develop a deeper understanding of my project. His feedback on my report was invaluable and really helped me to develop my report writing skills.

I am also very thankful to Dr Marko Pavlovic for taking the time to peruse my work and question me to think more about the practical applications of my work. This indeed broadened my scope of thinking and helped me realise the use cases of my work.

Much love to my pillars of support, mother and father, for believing in me throughout my masters. My sister for being the best and most amazing morale booster who kept reminding me that there is no excellence without labour. Lastly, it would be incomplete without mentioning my gratitude to all my friends with whom I have shared this bittersweet masters journey.

Siddhesh G. Rajadhyaksha
Delft, November 2020

Abstract

This era of science and technology has seen widespread use of composite materials for a variety of applications ranging from the defense sector to the transport and construction sectors. Composites are mainly comprised of fibres impregnated with a polymeric matrix and have a superior strength to weight ratio as compared to traditional construction materials like concrete and steel. The strength of the fibres is much larger than that of the matrix. Also, the fibres exhibits elastic brittle behaviour while the matrix shows a nonlinear plastic behavior before damage occurs. Thus the overall response of the material is subjective to which direction it is loaded. In reality a multitude of stresses act simultaneously on any structure and it is quite challenging to develop a constitutive formulation for the composite material that can predict the stresses in these mixed modes accurately.

This thesis aims at providing an improved constitutive formulation for the prediction of the material behavior of unidirectional composites. The constitutive formulation builds up on the existing knowledge of an isotropic invariant based yield function. The motive is to improve the performance of this constitutive law for better predicting the behavior under combined stress states, particularly in the presence of fibre stresses. Even thought the fibres behave completely elastic, the matrix surrounding the fibres is much weaker and tends to deform inelastically. The moment at which the yield stresses are developed in the matrix is also dependant on the level of stress in the fibres. To capture this behavious, two different yield criterion are formulated and testing in this project.

First an additive split of the stress tensor helps to separate the fibre and matrix stress components along the fibre('1') direction. The fibre stress is always elastic whilst the matrix stress component can behave inelastic. This matrix stress component is taken into account in the new constitutive laws. The first constitutive law is a modified version of the transversely isotropic invariant formulations as proposed by Vogler et al. [28] and the second constitutive law is an anisotropic yield function proposed by Tsai and Wu [25]. The invarants are reformulated with the matrix stress tensor while keeping the same functional form as that of the transversely isotropic invariant formulation . Again, the split in stress tensor is performed and used in association with the anisotropic yield function. The derivations of all the constitutive relations is presented extensively in the third chapter.

Followed by the formulations is the calibration of both the constitutive laws using the hardening curves derived from the micromodel simulations. The micromodel serves as the equivalent experimental test setup for the mesomodels presented in this project. Calibration of the mesomodels is a complex task in itself and the various trials were performed to determine the yield stress parameters that calibrate the models. Having calibrated the models, both the mesomodels are subjected to basic load cases and combined load cases. The MTIF model gives more consistent results than the TW model, however TW model performs better in the combined stress state of longitudinal axial tension and longitudinal in-plane shear.

Finally, the effect of the fibre stresses on the plastic behavior of the matrix is being captured but to different extents in both the models. Neither of the models is able to match the micromodel results for all simulations. The sensitivity of the yield stress parameters is brought to light and are the main cause for the overestimating behavior of the TW model. Lastly, all the observations were concluded followed by some recommendations for the future work.

Contents

List of Figures ix

List of Tables xi

1 Introduction 1
- 1.1 General Overview . . . 2
- 1.2 Motivation and Aim of the Research . . . 3
  - 1.2.1 Motivation . . . 3
  - 1.2.2 Aim of the Research . . . 4
- 1.3 Research Methodology . . . 4
- 1.4 Thesis Outline . . . 5

2 Background Information 7
- 2.1 Theory . . . 8
  - 2.1.1 General Overview of Material behaviour . . . 8
  - 2.1.2 Governing Equations of Plasticity . . . 8
- 2.2 Literature Review . . . 10
  - 2.2.1 Macroscale Failures . . . 10
  - 2.2.2 Constitutive model for mesoscale . . . 11
  - 2.2.3 Constitutive models for microscale . . . 16
- 2.3 Summary . . . 16

3 Constitutive Formulations 17
- 3.1 Modified Transversely Isotropic Invariant Formulation . . . 18
  - 3.1.1 Stress Separation . . . 18
  - 3.1.2 Modified yield function . . . 19
  - 3.1.3 Modified Flow Rule . . . 20
  - 3.1.4 Return Mapping . . . 21
  - 3.1.5 Consistent Tangent Operator . . . 24
- 3.2 Tsai Wu Yield Function . . . 25
  - 3.2.1 Context . . . 25
  - 3.2.2 Yield Function . . . 26
  - 3.2.3 Return Mapping . . . 26
  - 3.2.4 Consistent Tangent Operator . . . 28
- 3.3 Summary . . . 29

4 Numerical Implementation 31
- 4.1 Finite Element Model for Microscale . . . 32
  - 4.1.1 Representative Volume Element . . . 32
  - 4.1.2 Periodic Boundary Conditions . . . 33
  - 4.1.3 Generation of Hardening Curves . . . 34
- 4.2 Finite Element Model for Mesoscale . . . 37
  - 4.2.1 Representative Volume Element . . . 37
- 4.3 Calibration of Yield Stress Parameters . . . 38
  - 4.3.1 MTIF Yield Function Calibrations . . . 38
  - 4.3.2 Tsai Wu Yield Function Calibrations . . . 39
- 4.4 Return Mapping Algorithm . . . 42

5 Results **45**
5.1 Validation of Model . . . 46
5.1.1 In-Plane Shear . . . 46
5.1.2 Compression Transverse Axial Stress . . . 46
5.1.3 Tension Transverse Axial Stress . . . 47
5.2 Combined stress states . . . 48
5.2.1 Combined Axial Fibre Direction Stress and In-Plane Shear . . . 48
5.2.2 Combined Axial Fibre Direction Stress and Transverse Axial Direction Stress . . . 49
5.2.3 Combined Axial Transverse Direction Stress and In-Plane Shear Stress . . . 49
5.2.4 Summary . . . 50

6 Conclusions and Recommendations **51**
6.1 Conclusions . . . 52
6.2 Recommendations . . . 54

Bibliography **55**

List of Figures

1.1 A schematic of the different scales of observation for an orthotropic laminate 2
1.2 Shear stress-strain curve for combined longitudinal shear and longitudinal axial tension for ($\sigma_{11}/\sigma_{12} \in [57, 29, 11, 6, 0]$), [27] 3
1.3 Stress distribution over the cross section of a composite beam subjected to bending . . 4

2.1 A plot of stress vs strain showing the elastic and plastic strains 9
2.2 A flow chart of the progressive failure modeling of laminates [13] 11
2.3 Failure surfaces in the principal stress space, coaxially with the hydrostatic axis $\sigma_0(\sigma_1 = \sigma_2 = \sigma_3)$. (a) Von Mises; (b) Tresca; (c) Drucker-Prager; (d) Modified Drucker-Prager/Modified Mohr-Coulomb [9, 10] 12
2.4 Tubular Specimen [21] 13
2.5 Cruciform Specimen [21] 13
2.6 Schematic representation of the yield surface in invariant space [28] 15

4.1 Cross sectional view of the microscale representative volume element 32
4.2 Discretized view of the microscale representative volume element 32
4.3 Schematic of micromodel RVE with local coordinate axes and periodic boundary conditions 33
4.4 Hardening curve for uniaxial tension in transverse (or '2') direction 35
4.5 Hardening curve for uniaxial compression in transverse (or '2') direction 35
4.6 Hardening curve for biaxial tension in transverse (or '2' and '3') directions 36
4.7 Hardening curve for biaxial compression in transverse (or '2'and '3') directions 36
4.8 Hardening curve for in-plane shear stress 36
4.9 Hardening curve for transverse shear stress 36
4.10 Hardening curve for the matrix stress(σ_{11}^m) in uniaxial tension under fibre (or '1') direction 37
4.11 Hardening curve for the matrix stress(σ_{11}^m) in uniaxial compression under fibre (or '1') direction 37
4.12 Micromodel RVE and Mesomodel RVE 37
4.13 Hardening curve for the matrix stress(σ_{11}^m) under biaxial tension in fibre (or '1') direction for t = 0.001mm 40
4.14 Hardening curve for the matrix stress(σ_{22}) under biaxial tension in transverse (or '2') direction for t = 0.001mm 40
4.15 Hardening curve for the matrix stress(σ_{11}^m) under biaxial tension in fibre (or '1') direction for t = 0.0286mm 40
4.16 Hardening curve for the matrix stress(σ_{22}) under biaxial tension in transverse (or '2') direction for t = 0.0286mm 40
4.17 Graphical representation of the return mapping algorithm 42

5.1 Stress strain curve for in-plane shear stresses in MTIF Mesomodel 46
5.2 Stress strain curve for in-plane shear stresses in TW Mesomodel 46
5.3 Stress strain curve for transverse axial stress(compression) in MTIF Mesomodel 47
5.4 Stress strain curve for transverse axial stress(compression) in TW Mesomodel 47
5.5 Stress strain curve for transverse axial stress(tension) in MTIF Mesomodel 47
5.6 Stress strain curve for transverse axial stress(tension) in TW Mesomodel 47
5.7 Shear stress-strain curve for combined longitudinal shear and longitudinal axial tension for ($\sigma_{11}/\sigma_{12} \in [0, 6, 11, 29, 57]$, from top to bottom) in MTIF model 48
5.8 Shear stress-train curve for combined longitudinal shear and longitudinal axial tension for ($\sigma_{11}/\sigma_{12} \in [0, 6, 11, 29, 57]$, from top to bottom) in TW model 48
5.9 Axial stress-strain curve for combined longitudinal axial tension and transverse axial tension for ($\sigma_{11}/\sigma_{22} \in [11, 6, 0]$ from left to right) in MTIF model 49

5.10 Axial stress-strain curve for combined longitudinal axial tension and transverse axial tension for ($\sigma_{11}/\sigma_{22} \in [11, 6, 0]$ from left to right) in TW model 49
5.11 Shear stress-strain curve for combined longitudinal shear and transverse axial tension for ($\sigma_{12}/\sigma_{22} \in [11, 2, 0]$ from bottom to top) in MTIF model 50
5.12 Shear stress-strain curve for combined longitudinal shear and transverse axial tension for ($\sigma_{12}/\sigma_{22} \in [11, 6, 0]$ from bottom to top) in TW model 50

List of Tables

4.1 Material properties of the fibres and matrix for the micromodel 33
4.2 Orthotropic material properties for the mesomodel 38
4.3 Summary of other calibration trials 42

1

Introduction

This chapter contains general information on composite materials, their benefits and use cases. It then addresses some of the difficulties which are faced in accurately modelling the physical behaviour of these materials which leads to the motivation and aim of the project. The research questions are defined and the methodology is explained with a short overview of the layout of the report.

1.1. General Overview

Composite materials are a combination of two materials that are amalgamated to produce a new material with enhanced properties. Fibre reinforced polymers (FRP) are the most widely used composites that are made of fibres combined with a binder material. Usually, the fibres are glass or carbon fibres and the binder material is a polymer(resin) matrix. Fibre mats, unidirectional or bidirectional fabrics and fibre filaments are types of fibre reinforcements that are possible in FRP. Along with different types of polymers, the possibilities of fibre reinforced composites are endless. The fibres have high stiffness, high strength and behave mostly elastic with brittle failure. On the other hand, the polymer has relatively weaker material properties with respect to the fibres and the response is mostly nonlinear. Thus the composite exhibits the non uniform or anisotropic material behaviour.

A major advantage of FRP is that the material can be tailored and manufactured for each design. In addition to their lightweight, high strength and good corrosion resistant properties, composites have found wide applications in the automotive and aerospace industries with the construction industry slowly catching on. Composites are used to make structural parts like aeroplane fuselages, parts of the aeroplane wings and automotive chassis. In recent years, pedestrian bridges and lock gates have also been made with composites. These designs are possible on the ability to predict the ultimate load and residual strength of these structures. However, these designs can be made more efficient with the ability to better predict the physical response of the material, especially the failure mechanisms. Due to the heterogeneous composition of the composite material, multiple failure mechanisms are possible. For this, the stress states in the material for general loading conditions, boundary conditions and loading histories need to be accurately predicted [28].

To study the stress states that determine the nature of the failure of mechanisms, the composition of the material at different scales should be understood [8]. Laminates are comprising usually of unidirectional(UD) plies laid in different orientations. The macroscale, which represents all the layers of the material, is where the global structural geometry is defined. This is where the ultimate strength or the ultimate bending moment capacity of the entire laminate is evaluated. Mesoscale is the intermediate scale representing the material as homogeneous for an individual ply. Interply and intraply material behaviour can be well represented at this scale. Lastly the microscale wherein the individual components, the fibres and matrix, are represented individually. Microscopic failures affected by the position of the fibres and the fibre-matrix interface can be studied here. A schematic of the different scales can be seen in *figure*1.1.

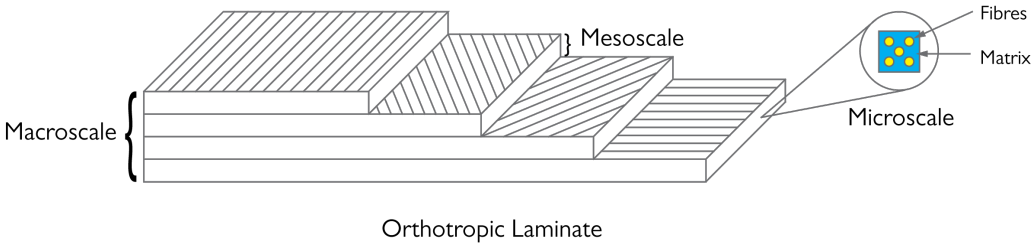

Figure 1.1: A schematic of the different scales of observation for an orthotropic laminate

In order to quantify the anisotropic material behaviour of composites, constitutive laws are implemented. The constitutive laws at microscale are fairly straightforward due to their limited input parameters as they are defined separately for the fibre and matrix. Microscopic models are often used in multiscale modelling to imitate the behaviour of laminates. In multiscale modelling, a finite element(FE) model is applied on both the macroscale and microscale. The stresses at the Gauss integration point of the macroscale are used as the boundary conditions for the microscale FE model. This requires the FE model to run twice in a simulation and is often referred as FE^2. Although this method yields accurate results, it comes with a very high computational cost which is not practical for engineering applications. On the other hand, mesoscale constitutive laws assume an individual ply to be homogeneous and are computationally less demanding. Nevertheless, the mesoscale constitutive laws are more complex as they have to capture all the microscopic phenomena and accurately represent them as a homogeneous ply. The input parameters for mesoscale constitutive laws should be chosen such

they are able to replicate all the trends of the microscopic material behaviour fairly accurately and at the same time use a reasonable number of experimental tests to define them [17].

Among the various constitutive model that have been proposed over the years[18, 19, 25, 28], a three dimensional transversely isotropic elastic-plastic constitutive law by Vogler et al. [28] for mesoscale has shown promise. Another study by Van Der Meer [27] validated this model with the help of micro-model simulations based on the constitutive laws proposed by Melro et al. [18]. This study revealed that although the transversely isotropic constitutive law is able to predict the elasto-plastic behaviour under individual stress states, it is unable to capture the influence of a combination of stress states under multi-axial loading. It is thus quite interesting to explore the possibilities to incorporate the interaction between the different stresses acting on the material.

This thesis focuses on using the knowledge of existing homogenized mesomodels to provide an improved constitutive law that is able to capture the interactions between stresses under multi-axial loading. The microscale models will be used as representative validation set for the mesomodel. The work will include the formulation of the equations governing the plastic behaviour of the material along with its numerical implementation. The results from this model will help us determine if the interaction between the stresses is successfully captured by the newer implementation.

1.2. Motivation and Aim of the Research

1.2.1. Motivation

Multiscale modelling has gained popularity in it's ability to predict the behaviour of composite materials accurately, however they come at a high computational cost. An alternative to this is the use of homogenization techniques that are able to reproduce the same physical effects for mesomodels. A novel approach proposed by Vogler et al. [28] with an invariant based formulation of the yield function is able to express the effects of different stress states reasonably for mesomodels. The invariant based formulation employs an invariant each for in-plane shear, transverse shear and uniaxial tension/compression and biaxial tension/compression stress states. As a result it is able to capture the effects of these stress states, however a study by Van Der Meer [27] revealed that the influence due to fibre direction stresses(σ_{11}) on the other stress states is not taken into account. It can be seen from *figure*1.2 where it is observed that for various fibre direction stresses the onset of plasticity in the in-plane shear stresses(σ_{12}) is affected.

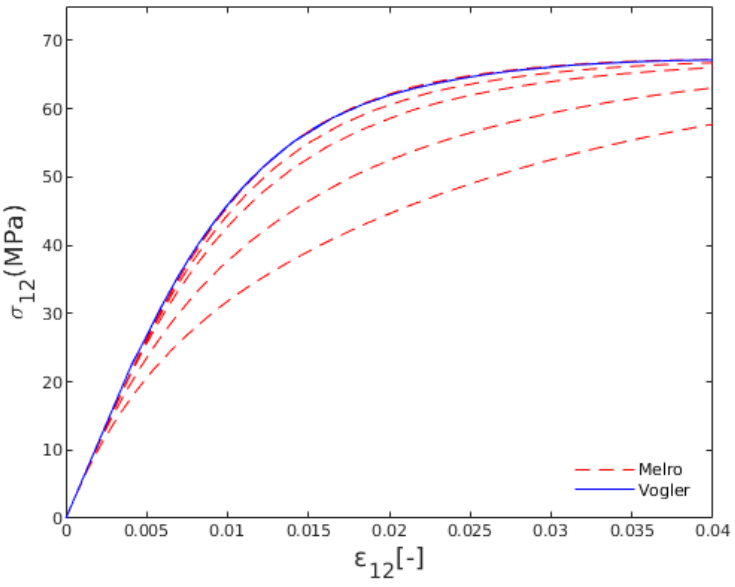

Figure 1.2: Shear stress-strain curve for combined longitudinal shear and longitudinal axial tension for ($\sigma_{11}/\sigma_{12} \in [57, 29, 11, 6, 0]$), [27]

These combination of stresses can be identified with the help of a simple beam example as shown in

figure 1.3. The beam is comprised of unidirectional laminates for the top and bottom flanges of the beam and is subjected to bending. The flanges predominantly carry the load in tension and compression but due to the variation of these stresses along the depth of the member, in-plane shear stress is developed at the interface between the plies of the laminate. Thus it is a realistic loading scenario and the effect of fibre direction stresses on the onset of plasticity should be taken into account. The main motivation of this project is to provide an improved constitutive model by incorporating the effect of fibre direction stresses on matrix plasticity.

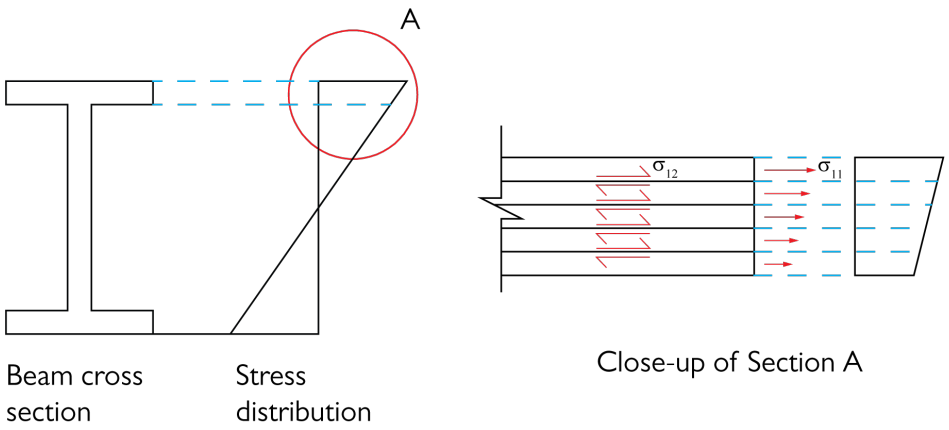

Figure 1.3: Stress distribution over the cross section of a composite beam subjected to bending

1.2.2. Aim of the Research

Laminated composites have different types of failure mechanisms as compared to traditional construction materials. Matrix cracking, delamination between plies and fibre ruptures are some of the common failure modes that are observed in laminated composites. To accurately predict these failure modes, it is crucial to understand the development of stresses not only near the failure surface but also in the surrounding material. The mesoscale is chosen as it is possible to study the stress states in this scale to evaluate the failure modes inside the material and the outside interface between plies. Since the existing homogenized mesomodels in their current form are unable capture all the interactions between different stress states, the failures cannot be accurately determined. Anisotropic yield criteria however, have more flexibility to account for different behaviours in different directions but are limited as they are difficult to calibrate for combined stress states. This thesis aims at improving an existing constitutive law which is based on a transversely isotropic invariant based formulation and an anisotropic formulation to better quantify the physical behaviour of the composite in multi stress state. The emphasis will be on overcoming the shortcoming of the existing models while maintaining it's simplicity. The scope of this project is limited to the inelastic behaviour of unidirectional composites just before damage occurs. The work will build upon the framework developed by Van Der Meer, for mesoscale modelling of UD composites [27] to incorporate the effects of fibre direction stresses on the matrix plasticity.

Research Questions

1. How to incorporate the effect of fibre direction stress(σ_{11}) on the evolution of plastic in-plane shear stress(σ_{12}) within the transversely isotropic invariant based yield criterion?
2. Would an anisotropic yield criterion be able to capture the effect of the fibre direction stresses(σ_{11}) on plastic behaviour of the matrix?
3. How sensitive is the anisotropic formulation to the calibration of the model?

1.3. Research Methodology

The methodology of this research can be divided into three parts, understanding the theoretical background, improving the constitutive model along with its numerical implementation and finally interpreting

the results. At first a small study of the general concepts of plasticity was carried out to fully understand the governing equations of plasticity. This exercise helped to gain insights into the implementations of constitutive laws for composite materials, presented in the literature. After a thorough literature review, the research questions were formulated. Improved formulations proposed by Van Der Meer in the transversely isotropic framework were investigated. Another formulation with the anisotropic yield function was also worked out. Then the numerical implementation of these governing equations of plasticity with finite elements, was carried out with the help of C++ JemJive package. Two different types of numerical models were analysed, first being the microscale model which in the scope of this project, served as a test setup and the second model was the homogenized mesoscale model. The micromodel results are assumed to be representative of the actual composite material behaviour and also used for generating input for the homogenized mesoscale model. The major focus of this thesis will be on the improved constitutive laws proposed and applied at mesoscale. Next the performance of these yield criteria are evaluated with respect to the micromodel and presented. Lastly, the conclusions of this study are summarized followed by recommendations for further improvement.

1.4. Thesis Outline

The structure of this report is aligned with the proposed methodology. *Chapter* 2 presents the necessary background information, which is an extensive literature review and a brief explanation of the general theory of plasticity. The transversely isotropic formulation from literature is explained in detail to help understand the working of that model. A newer formulation along with a new yield criterion is presented in *Chapter* 3. This chapter also describes the numerical implementations of the newer formulations. *Chapter* 4 will explain the representative volume elements used for the finite element simulations of both the microscale and mesoscale models. *Chapter* 5 presents the results of newer implementations on the mesomodel which is compared with the micromodel results for different combined load cases. The results will help us realise the impact of the newer implementation on the including the fibre direction stresses on the matrix plasticity. Lastly, *Chapter* 6 will conclude the findings of this thesis and suggest the recommendations for future research.

2

Background Information

This chapter aims to familiarize the reader with the general notations of plasticity and briefly describe the theory of plasticity. A broad literature review which talks about the failures mechanisms of composites. Analytical techniques in correlations with their experimental setups have been discussed. This helps to strengthen the research questions and leads to the main formulations of this project.

Before starting the main constitutive formulations, it is important to know what plasticity is and how the constitutive relations are used to incorporate nonlinear material behaviour. The general theory presented in this chapter addresses the theory of plasticity which helps understand how the plastic nonlinearity in materials is formulated. In the second section of this chapter, the knowledge on constitutive modelling is build up from the reviewed literature is presented. This will help lay the ground work for the following chapters.

2.1. Theory

2.1.1. General Overview of Material behaviour

A material subjected to increasing load deforms linearly proportion to the load upto a certain limit after which it deforms nonlinearly. This limit of linearly proportional deformations is know as elastic limit and these deformations upto the elastic limit can be recovered upon removal of the load. The nonlinear deformations are called inelastic or plastic deformations and cannot be recovered upon the removal of loads. Materials that have sufficient capacity to show plastic deformations before failure are called ductile materials where as materials that do not show any significant plastic deformations are called brittle materials. Common metals like steel are ductile whereas materials like cement or concrete are brittle.

The relationship that relates the elastic strains to the elastic stresses is known as Hooke's law. The amount of stress for unit strain in the material is known as the elastic modulus of that material. These properties are different in different directions and vary between materials. In general, materials can posses different properties in different directions depending on their composition. Such materials are known as anisotropic materials and behaves differently in each direction. A case where the material properties can be described completely along 3 orthogonal directions are known as orthotropic materials. Another subset of orthotropic materials are isotropic materials, where the property of the material is same along all three directions. Also a special case where the material property is same along only two directions and differently along the third direction are called transversely isotropic materials. Metals are a good example of isotropic materials whereas UD fibre reinforced composites are examples of transversely isotropic materials.

All the different properties pertaining to their respective directions are collected in the form of a tensor. When computing the stresses from the strains this tensor is called the stiffness matrix. The inverse of this matrix is called the compliance matrix and can be used to compute the strains from the stresses. These tensors are what form the constitutive relationships for each material. This tensor can be easily defined for elasticity, although, additional equations are required to define this tensor for plasticity.

2.1.2. Governing Equations of Plasticity

Any problems in static mechanics is solved in a formal fashion with the help of kinematic equations, constitutive equations and equilibrium equations. The kinematic equations relate the body displacements to the internal strains in the material. The constitutive equations relate the internal strains to the internal stresses. Finally the equilibrium equations are used to balance the internal forces(stresses) in the body with the external forces(stresses) applied to the body. The constitutive equations in it's most general form can be seen in *Eq.*2.1 where σ is the second order stress tensor, ε is the second order strain tensor and $\mathbf{D}$ is the fourth order tensor often called the stiffness matrix. For elastic loading, this relation is linear(also known as Hooke's law) but for plastic loading it is nonlinear. The stiffness matrix is where the material nonlinearity is incorporated.

$$\sigma = \mathbf{D}\varepsilon \tag{2.1}$$

To define the correct stiffness matrix for accurately calculating the stresses under nonlinear plastic loading, the theory of plasticity is followed. Plasticity can be represented by three major ingredients, a yield criterion, a flow rule and the consistency conditions[1, 6, 23, 24]. Generally the yield criterion is a scalar function of the stress tensor and a plastic internal variable. A general form of the yield function can be seen in *Eq.*2.2 where κ is the plastic internal variable. The yield function represented in 3D space, defines a yield surface that bounds the stress states that can exist in a material at any given time. According to theory, a stress state cannot exist outside the yield surface, but it can still exist on

the yield surface itself. The stress states inside the yield surface are elastic and the ones that exist on the surface are plastic.

$$f(\sigma, \kappa) \leq 0 \tag{2.2}$$

The deformations are quantified by elastic strains and plastic strains as shown in *Eq.* 2.3. The elastic strains are strains that can be recovered on unloading at any given time. The theory of plasticity assumes the unloading to always follow Hooke's Law(*Eq.*2.4) and thus these strains can be easily determined. With the total strains known and computed elastic strains, it is possible to determine the plastic strains (*Fig.*2.1). Nevertheless, this procedure is not as effortless as it seems. To correctly determine the elastic strains, it is crucial to know the correct state of stress in the material at a given time. When solving a problem of static mechanics, the stresses need to be computed from strains, as a result there exists an implicit problem where the stresses are unknown.

$$\varepsilon = \varepsilon^e + \varepsilon^p \tag{2.3}$$

where, ε^e is elastic strains and ε^p are plastic strains

$$\sigma = \mathbf{D}_e \varepsilon_e \tag{2.4}$$

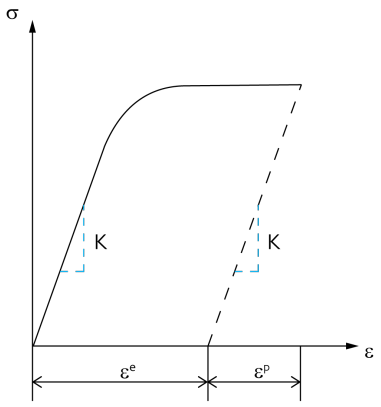

Figure 2.1: A plot of stress vs strain showing the elastic and plastic strains

A common technique used to solve this problem according to theory of plasticity is to assume a functional form of the plastic strains. It states that the plastic strains can be determined as a product of a plastic multiplier and a flow rule. The plastic multiplier ($\dot{\gamma}$) is a scalar quantity, determines the magnitude of the plastic strain and the flow rule (m) is a tensor that dictates the plastic flow direction, shown in *Eq.*2.5. Two types of flow rules exist, one is the associative flow rule wherein the flow rule is defined to be the gradient to the yield function and non associative flow rule where the flow rule is the gradient to a plastic potential function. The plastic potential function usually has a similar form as that of the yield function and is chosen where the the associative flow rule does not hold good for predicting the plastic phenomena.

$$\varepsilon^p = \dot{\gamma} \cdot m \tag{2.5}$$

Lastly, the consistency conditions are obtained from the loading unloading conditions postulated by Kuhn-Tucker which can be seen in *Eq.*2.6. These can be understood with the help of a simple example. Clearly, if a stress point is elastic, it will satisfy $f \leq 0$ and the plastic multiplier is $\dot{\gamma} = 0$. Subsequently, if

a stress point is plastic, it has to lie on the yield surface thus satisfying $f = 0$ and plastic strains $\dot{\gamma} > 0$. As a result, in both cases the product of f and γ is equal to zero.

$$f \leq 0\ ,\ \dot{\gamma} \geq 0\ ,\ f\dot{\gamma} = 0 \tag{2.6}$$

With a functional form of the yield function and flow rule, all the above elements can be combined to derive a tangential stiffness matrix that gives the relation between the strains and stresses at each local integration point. Once this stress strain relationship is known, the problem at global scale which is to balance the sum of internal forces with the sum of external forces acting on the body can be solved. In essence this sums up the underlying theory behind a non-linear finite element code dealing with plasticity.

2.2. Literature Review

Fibre reinforced polymer composites have wide applications in aerospace, automobile and construction industry, due to their lightweight, high stiffness and high strength. They are used to manufacture various structural components and thus it is crucial to be able to determine the resistance capacity of these structures. In order to determine the resistance capacity, we need to know the exact material behaviour. Since FRP material are laminar and inhomogeneous, their material behaviour is very difficult to predict. Various approaches to predict this material behaviour will be discussed in the following subsections.

2.2.1. Macroscale Failures

Composite laminates are heterogeneous materials that are made by stacking of multiple plies on each other and bonded with an adhesive. Due to the laminar nature of the material, the failure of the laminates is complex and dependent on the failure of the ply and the interface between the plys. A variety of failure modes like matrix cracking, delamination and fibre rupture are observed on ply level. To estimate these failures, progressive failure modelling techniques have been proposed by Camanho et al. [3], Chang and Chang [5], Hahn and Tsai [13], Liu and Tsai [15], Maimí et al. [17], Van Der Meer and Sluys [26]. The modelling procedure comprises of two main parts, first is the failure of a ply depending on the stress state in it and second is a degradation condition that incorporates the impact of the ply failure on the overall laminate properties.

For simplicity, the ply is considered as homogeneous and regarded to have linear behaviour along the fibre direction(σ_{11}) and nonlinear behaviour in the other directions. The origins for nonlinearity in a ply are attributed to the nonlinear behaviour of the polymeric resins used to make them. To model the failure of a ply, a stress-strain relationship is required. Two most commonly used relations are the ones proposed by Tsai and Wu [25] and Hahn and Tsai [13]. They are admired due to their ease of implementation as they have limited inputs parameters that can be quantified with the help of experiments. The nonlinear stress-strain relationship proposed by Hahn and Tsai [13] is shown in *Eq.*2.7.

$$\gamma_{12} = \frac{1}{G_{12}}\sigma_{12} + \beta\sigma_{12}^3 \tag{2.7}$$

where,

G_{12} is the initial ply shear modulus
β is an experimentally defined constant

This criterion is adopted by Chang and Chang [5] and combined with property damage model where the properties of the ply are degraded if they are damaged. These models combined will dictate how the overall laminate will fail. Open circular hole specimens have been numerically modelled by Chang and Chang [5] with this criterion and validated with experimental results to show its capability in predicting the uniaxial strength of the laminates. Although, it can be seen from the equation 2.7, the failure of the ply is associated with the shear capacity of the ply, which is not always true. In reality, other stresses also have an impact on the failure of the ply. A modification of this criterion is presented in Camanho et al. [2] which tries to incorporate the effect of transverse stress through a modified β parameter. The

modification suggests a new value of $\beta + \sigma_{22}/\chi$ instead of β when $\sigma_{22} \geq 0$. Although this representation is better, it is still not a general constitutive law [17].

$$F_i\sigma_i \; + \; F_{ij}\sigma_{ij} \; = \; 1 \tag{2.8}$$

where i,j = 1, 2 …6.

Another general model for defining the nonlinear stress strain behaviour of anisotropic materials is given by Tsai and Wu [25]. Also known as the quadratic failure criterion, it comprised of two strength tensors, F_i and F_{ij} and two stress tensors σ_i and σ_{ij} is shown in *Eq.*2.8. This is a scalar representation is used by Hahn and Tsai [13] and Van Der Meer and Sluys [26] in their progressive damage models. The approach taken by Hahn and Tsai [13] is more traditional where the yield criterion is used in tandem with a degrading damage model to evaluate the capacity of the laminate. A general idea of ply-by-ply progressive failure modelling followed in [13] can be seen in *figure*2.2. This study revealed that it is possible to interpolate and extrapolate the strengths of combined stresses where data is not available provided the input data is good. The ability to correctly determine the input parameters has an important impact on determining the behaviour of the ply.

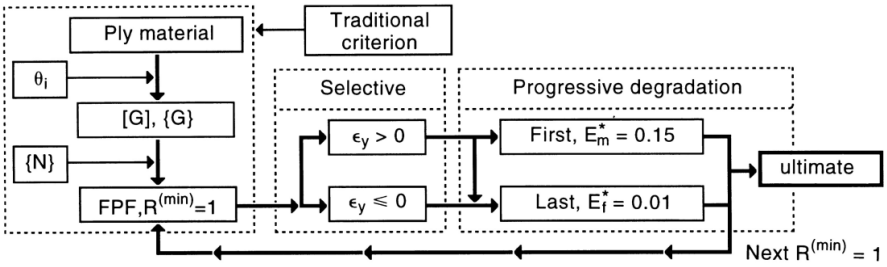

Figure 2.2: A flow chart of the progressive failure modeling of laminates [13]

A different use of the Tsai and Wu yield criterion can be found in the works of Van Der Meer and Sluys [26] where a softening plasticity is applied on the yield surface to simulate the damage of a ply. This is done by introducing linear isotropic softening which is the shrinking of the yield surface. The uniaxial strength parameters are multiplied with a factor $h(\kappa)$, where κ is a state variable. The slightly different form of the yield surface is presented in *Eq.* 2.9. Even though the model can capture different sequentially occurring mechanisms, it encounters some problems in calibration. It concluded that this is a trait of the homogenization of the constitutive models.

$$f(\sigma, \kappa) = \frac{1}{2}\sigma \cdot F_{ij}(\kappa) \cdot \sigma + F_i(\kappa) \cdot \sigma - 1 = 0 \tag{2.9}$$

with

$$F_{ij}(\kappa) = \frac{1}{h(\kappa)^2}F_{ij}, \quad F_i(\kappa) = \frac{1}{h(\kappa)}F_i \tag{2.10}$$

It can inferred that the constitutive models used for a ply significantly affect the fidelity of the progressive damage models. Difficulty in calibration, ability to accurately determine the input parameters and generality are some of the existing difficulties faced by existing constitutive models. Thus more investigation is needed into how these ply constitutive models are formulated. We need to look further as to what difficulties are associated with constitutive modelling and where they arise from.

2.2.2. Constitutive model for mesoscale

Intrinsic Material Properties of Polymer Matrix

Developing constitutive laws for composite plies is quite elaborate as the material is not homogeneous. The matrix in it's plane state is quite homogeneous but due to the presence of fibres in the matrix, the

matrix behaviour is altered drastically. To get a general idea, the constitutive models proposed for plane unreinforced resins are discussed briefly.

A study by Pae and Rhee [22] revealed that the response of the matrix is sensitive to the hydrostatic pressure on it. Keeping this in mind it is important to choose a yield criterion that is pressure sensitive. Most common pressure sensitive yield criteria present in literature are the ones proposed by Mohr-Coulomb and Drucker-Prager [6]. The works of Fiedler et al. [9] and Ghorbel [10] have used the modified version of Mohr-Coulomb and Drucker-Prager yield criterion respectively to estimate the response of the matrix. The modifications are done to transform the yield surface to an open parabolic surface while still maintaining it's pressure sensitive nature. The various failure surfaces are shown in *figure* 2.3 where σ_1, σ_2 and σ_3 are the principal stress axis.

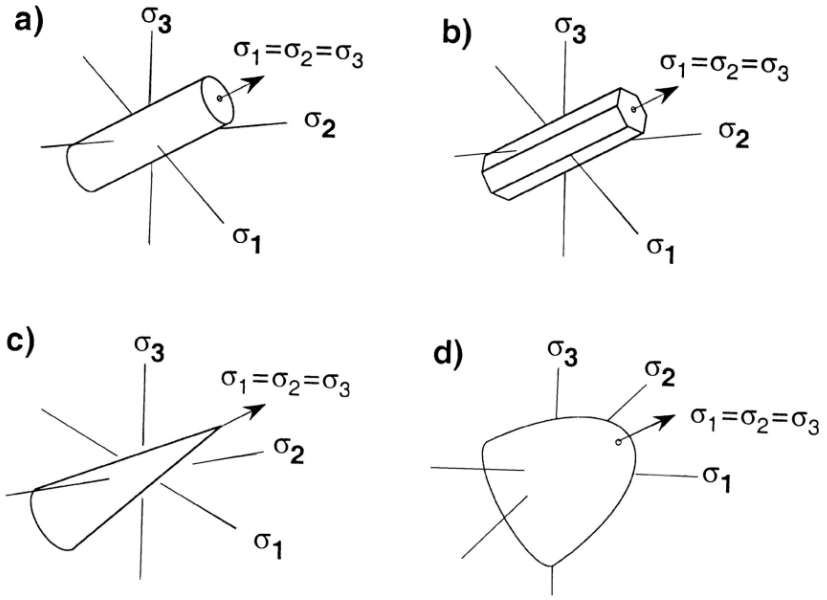

Figure 2.3: Failure surfaces in the principal stress space, coaxially with the hydrostatic axis $\sigma_0(\sigma_1 = \sigma_2 = \sigma_3)$. (a) Von Mises; (b) Tresca; (c) Drucker-Prager; (d) Modified Drucker-Prager/Modified Mohr-Coulomb [9, 10]

A salient feature of pressure sensitive yield criteria is to differentiate the material response for tensile and compressive pressures. The closed end of the parabolic yield criteria bounds the tensile stresses in the matrix whilst the compressive stresses are unbounded. This is fine since the matrix has poor capacity in tension as opposed to it's capacity in compression.

A few cursory studies have shown that the modulus of the polymer starts to degrade with the increase in temperature [7, 20, 29]. This occurs because the cross links in the polymer chains start to disintegrate. The temperature at which the modulus starts to drop is known as glass transition temperature(θ_g). A constitutive model developed by Dupaix and Boyce [7] shows that degradation is a rate dependant process. The model showed good correlation with experimental results for polyethylene terephthalate-glycol(PETG) at temperatures of glass transition(reference taken at 73°C) and above. Although this phenomenon is important, we are more interested in the mechanical response of the constitutive law which was not investigated in here.

Experimental Limitations

Constitutive equations are formulated to analyse the relationship between stresses and strains for a given loading. Experimental setups subjected to similar loading conditions are needed to justify these equations. The feasibility of the experimental test setups often decide the scope of the research. Hence it is important to know the different types of experimental setups available for testing a particular loading case. A paper by Olsson [21] reviews different methods for testing composite specimens subjected to multi-axial in-plane loading and out of plane loading. Cruciform and tubular test specimens as shown

in *figure* 2.4 and 2.5 are employed for biaxial loading scenarios. A tubular specimen is fixed on both ends and biaxial load is applied with the combined action of twisting and tension or compression. The tubular specimens needs to be internally pressurized to yield good results. In a cruciform specimen, the end fixtures are either two actuators and two fixed ends or all four actuators. The biaxial stresses are unevenly distributed when only two actuators are used whereas even stress distribution occurs in the specimen with four actuators.

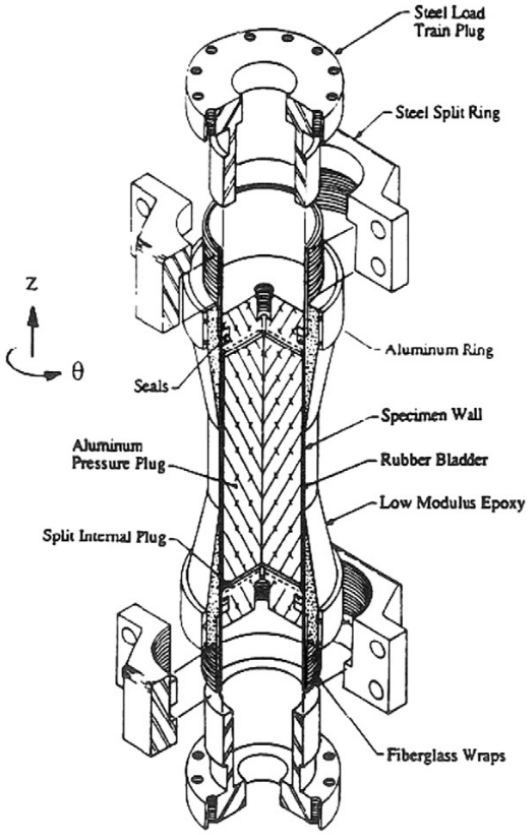

Figure 2.4: Tubular Specimen [21]

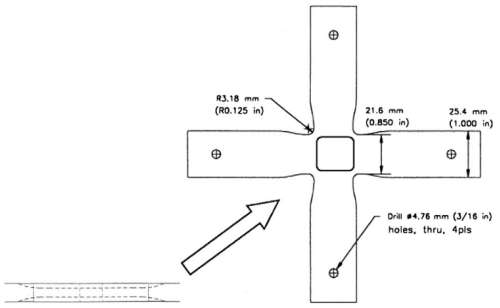

Figure 2.5: Cruciform Specimen [21]

Off-axis specimens and angle-ply specimens are two types of tests where the fibre direction is not aligned with the direction of primary loading. Due to the deformation incompatibility at the loading clamps, the fidelity of these tests are limited to a certain range of biaxial stress states. Out of plane axial loading and bending tests are conducted to observe interlaminar stresses. The tests are more straightforward however there is a need to employ thick plys to appropriately capture the interlaminar stresses. In short, there are significant problems in determining the strength of composite laminates in multi-axial loading. Also, the test setups are quite complicated and the specimens are expensive to manufacture. A solution is to develop a multiaxial failure criteria based on the data available from the existing test samples without the need for developing new experimental test setups[21].

Constitutive Models

Considering the various factors of intrinsic material properties and experimental limitations it is indeed quite difficult to form a robust constitutive law for composites. Modified versions of existing yield functions have been used in various studies [2, 5, 9, 10, 13, 17] but each with their own constrains. The criterion by Hahn and Tsai [13] considers only the in-plane shear stresses(σ_{12}) to define the yield surface. Camanho et al. [2] and Maimí et al. [17] have tried to incorporate the effect of transverse directions stresses(σ_{22}) and transverse strains(ε_{22}) respectively, in addition to in-plane shear. None of these explain the complete stress state of the material in their yield criteria. However, the yield criteria by Tsai and Wu [25] and Vogler et al. [28] are two formulations that fully take into account the complete stress

state.

Tsai-Wu Yield Criterion
One of the earliest proposed constitutive models for anisotropic materials was the one presented by Tsai and Wu [25]. It is still popular for it's operational simplicity as it utilizes two strength tensors(F_i and F_{ij}) along with the linear and quadratic presence of the stress tensor to form a scalar yield function(*Eq.*2.8). The linear stress tensor(σ_i) contains all the individual stress states in a three dimensional space and is a vector with 6 components. The quadratic stress tensor(σ_{ij}) contains a combination of all the 6 individual stress states and forms a symmetric 6x6 matrix. The strength tensor F_i along with σ_i takes into account the effect of the individual stress states whereas the strength tensor F_{ij} along with σ_{ij} takes into account the interactions between these individual stress states on the yield criteria. An advantage of this is that each interaction can be controlled with the respective strength tensor components. The off-diagonal terms of the strength tensor F_{ij} are the parameters for interacting stresses.

$$F_{ii}F_{jj} - F_{ij}^2 \geq 0 \tag{2.11}$$

Since the yield function is scalar, it is automatically invariant and the strength tensors should follow rules of transformation. In addition, a stability condition(*Eq.* 2.11) is imposed to keep the yield surface a closed ellipsoidal. The components of the strength tensors can be reduced by considering material symmetries which results in the components of the strength tensor being either eliminated or dependant on other strength quantities. Because of this flexibility, it is widely used for evaluating laminate behaviour [13, 26]. Despite it's simplicity, the calibration of the off-diagonal parameters of the strength tensor is susceptible to the experimental results of combined stress states.

Transversely Isotropic Invariant Based Yield Criterion
The model formulated by Vogler et al. [28] is able to represent the nonlinear behaviour of the UD composites under multiaxial loading. This is accomplished with a transversely isotropic invariant based yield criterion along with a non associative flow rule. The yield function(see *Eq.*2.12) is comprised of strength parameters α's and invariants I with each invariant identifying a particular stress state. The effect of transverse shear, in-plane shear and biaxial loading are independently gauged by I_1, I_2 and I_3 respectively for the yielding of the model. Due to the linear behaviours of fibres, the fibre direction stresses(σ_{11}) are kept out of the plasticity inducing stresses.

$$f\,(\sigma, \bar{\varepsilon}^p, A) = \alpha_1 I_1 + \alpha_2 I_2 + \alpha_3 I_3 + \alpha_{32} {I_3}^2 - 1 \leqslant 0 \tag{2.12}$$

with

$$\begin{aligned} &\alpha_3 = \alpha_3^t \;\; \alpha_{32} = \alpha_{32}^t \quad \text{if } I_3 > 0 \quad \text{and} \\ &\alpha_3 = \alpha_3^c \;\; \alpha_{32} = \alpha_{32}^c \quad \text{if } I_3 \leqslant 0 \end{aligned} \tag{2.13}$$

In order to account for the asymmetrical response of the composite in positive pressure and negative pressure, different α_3 and α_{32} values are implemented. This results is a parabolic yield surface that can be plotted uniquely in the invariant space shown in *figure* 2.6. One more crucial ingredient in this model is the non associative flow rule as shown in *equation* 2.14, controls the direction of plastic flow.

$$g(\sigma, A) = \beta_1 I_1 + \beta_2 I_2 + \beta_3 I_3^2 - 1 \tag{2.14}$$

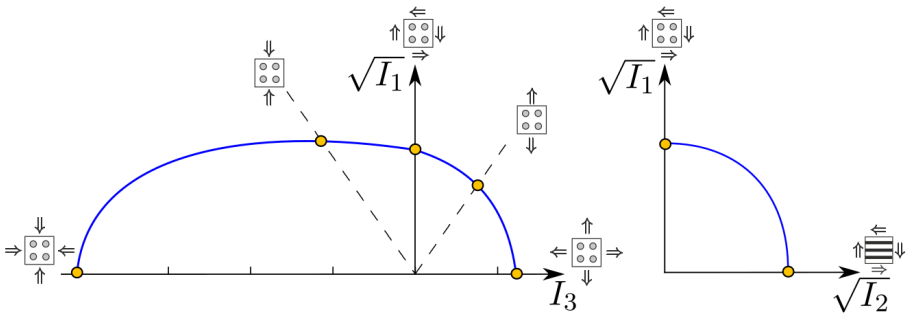

Figure 2.6: Schematic representation of the yield surface in invariant space [28]

These constitutive formulations are implemented with the help of an Euler backward scheme to calculate the plastic strains and stresses. The general form of the yield function and flow rule are presented in *Eq.* 2.15 and *Eq.* 2.18 are implemented with the help of a UMAT subroutines in Abaqus.

$$f(\sigma, \bar{\varepsilon}^p, A) = \frac{1}{2}\sigma : \mathbb{K} : \sigma + \mathbb{L} : \sigma - 1 \leqslant 0 \tag{2.15}$$

where,

$$\mathbb{K} = \begin{bmatrix} 0 & 0 & 0 & 0 & 0 & 0 \\ 0 & 2\alpha_{32} + \frac{1}{2}\alpha_1 & \alpha_{32} - \frac{1}{2}\alpha_1 & 0 & 0 & 0 \\ 0 & 2\alpha_{32} - \frac{2}{3}\alpha_1 & \alpha_{32} + \frac{1}{2}\alpha_1 & 0 & 0 & 0 \\ 0 & 0 & 0 & 2\alpha_2 & 0 & 0 \\ 0 & 0 & 0 & 0 & 2\alpha_1 & 0 \\ 0 & 0 & 0 & 0 & 0 & 2\alpha_2 \end{bmatrix} \tag{2.16}$$

and

$$\mathbb{L} = \begin{Bmatrix} 0 & \alpha_3 & \alpha_3 & 0 & 0 & 0 \end{Bmatrix}^T \tag{2.17}$$

$$g(\sigma, A) = \frac{1}{2}\sigma : \mathbb{M} : \sigma - 1 \tag{2.18}$$

where,

$$\mathbb{M} = \begin{bmatrix} 0 & 0 & 0 & 0 & 0 & 0 \\ 0 & \frac{1}{2}\beta_1 + 2\beta_{32} & -\frac{1}{2}\beta_1 + 2\beta_2 a & 0 & 0 & 0 \\ 0 & -\frac{1}{2}\beta_1 + 2\beta_{32} & \frac{1}{2}\beta_1 + 2\beta_{32} & 0 & 0 & 0 \\ 0 & 0 & 0 & 2\beta_2 & 0 & 0 \\ 0 & 0 & 0 & 0 & 2\beta_1 & 0 \\ 0 & 0 & 0 & 0 & 0 & 2\beta_2 \end{bmatrix} = \begin{bmatrix} 0 & 0 & 0 & 0 & 0 & 0 \\ 0 & 1 & -\nu^p & 0 & 0 & 0 \\ 0 & -\nu^p & 1 & 0 & 0 & 0 \\ 0 & 0 & 0 & 2\,(1+\nu^p) & 0 & 0 \\ 0 & 0 & 0 & 0 & 2\,(1+\nu^p) & 0 \\ 0 & 0 & 0 & 0 & 0 & 2\,(1+\nu^p) \end{bmatrix} \tag{2.19}$$

Even though it's merits, this model fails to take into account the effect of fibre direction stresses on the matrix plasticity as shown by Van Der Meer [27]. This can be seen with the help of *figure* 1.2 from *Chapter* 1. The figure displays how the shear stresses in the matrix go into plasticity sooner for high ratios of fibre stress to shear strain values. These observations are made by comparing the results from this model to the results of a microscale model developed by Melro et al..

2.2.3. Constitutive models for microscale

Over the years, microscale models have gained demand due to their higher accuracy in predicting composite behaviours. In a typical micro model, the fibres and matrix are modelled independently along with a fibre matrix interface. A number of studies have been performed with micromodels by [4, 11, 18, 19]. Micro models are often used in multiscale modelling [8, 14] where the macroscale model are linked to a micro model at each integration point. The strains at the macroscale integration point are used as boundary conditions of the micromodel. Due to accurate prediction of the stress strain relationship from the micromodel, the performance of the macromodel is improved. Another application of the micromodel is to generate virtual test samples for mesomodel as is done in [27]. However, the micromodels are computationally very heavy.

$$\Phi\left(\sigma, \sigma_c, \sigma_t\right) = 6J_2 + 2I_1\left(\sigma_c - \sigma_t\right) - 2\sigma_c\sigma_t \tag{2.20}$$

$$g = \sigma_{\mathrm{vm}}^2 + \alpha p^2 \tag{2.21}$$

The work of Melro et al. [18] is focused on the nonlinear epoxy matrix behaviour and interface between the fibres and matrix. A thermodynamically consistent elasto-plastic damage model is developed with cohesive elements to model the interface. Looking closely at the yield criterion(*Eq.* 2.20), the J_2 invariant captures the effect of deviatoric stresses but in order to make the yield criterion a function of pressure, the I_1 invariant is added. Two internal variables of σ_c and σ_t are introduced to take into account the different behaviour of the matrix in compression and in tension. This results in a paraboloidal yield surface in 3D stress space. These internal variables also incorporate hardening in the model and with a non associative flow rule (*Eq.* 2.21), the overall inelastic behaviour of the epoxy matrix is accurately predicted. Thus, this model provides a reliable source for validating analytical models and serves as a virtual test setup.

2.3. Summary

From the above literature review, it can be said that the success of predicting the behaviour of laminates relies heavily on the accuracy of the ply constitutive models [2, 5, 13, 15, 26]. These ply constitutive models suffer from the intrinsic material properties of the matrix material which is sensitive to temperature and pressure [7, 20, 22, 29]. Some constitutive models are limited due to lack of experimental data [13, 25] whilst other models lack generality as they only consider few stresses to be responsible for inelastic behaviour [2, 13, 17]. The constitutive laws proposed by Tsai and Wu [25], Vogler et al. [28] are more general and consider the influence of all the stresses in the continua. Multiscale modelling on the other hand has gained popularity and yields reliable results however the computational time for such models is very high.

With the desire to have better analytical models to predict overall laminate behaviour, there is need for better constitutive properties at ply level. Even though the multiscale modelling approaches have good results, their cost of computation is very demanding so the need for homogenized ply models still stand. The yield criterion proposed by Vogler et al. [28] and Tsai and Wu [25] show promise and can be improved. Taking into account the difficulties in experimental setups [21], for the purpose of this thesis, the results of the microscale model [18] will be considered representative of the actual composite material behaviour.

3

Constitutive Formulations

This chapter contains all the constitutive formulations for deriving the nonlinear plastic relationship between strains and stresses. Two different yield functions are presented along with their respective flow rules. Finally the consistent tangent operator for both cases is derived in order to incorporate it into the numerical framework.

For improving the nonlinear response of homogenized mesoscale models, a better constitutive law is needed. The constitutive laws comprise mainly of the yield functions and the plastic potential function. The yield function helps to determine if the material behaves elastic or plastic where as the plastic potential function dictates the direction of plastic flow. This chapter will present the new formulations that were developed in this thesis project.

First, the fibre and matrix stresses in the fibre direction('1' direction in local coordinate frame) are considered separately for the mesoscale models. Then an improved form of the transversely isotropic invariant based yield function developed by Van Der Meer is explained in the first section. On the basis of this framework, in the next section a yield function as proposed in Tsai and Wu [25] is used along with an associative flow rule to determine the nonlinear response of the mesomodel.

3.1. Modified Transversely Isotropic Invariant Formulation

3.1.1. Stress Separation

Before beginning the new formulation of the constitutive equations for mesomodel, the yield function proposed in the paper by Vogler et al. [28] is briefly explained. The yield function is as shown in *Eq.* 3.1, is comprised of three invariants, each representing a particular stress state. The simplified form of the invariants in *Eq.* 3.2 shows that I_1 describes the transverse shear stress, I_2 the in-plane shear stress and I_3 the biaxial stress or pressure. The fibre direction stress σ_{11} is left out from the invariants and correspondingly the yield function. The flow rule is also comprised of the same invariants and thus lacks the influence of fibre direction stress. As a result, the effect of fibre direction stress on matrix plasticity is not captured as revealed in the study by Van Der Meer [27].

$$f\left(\sigma, \bar{\varepsilon}^p, A\right) = \alpha_1 I_1 + \alpha_2 I_2 + \alpha_3 I_3 + \alpha_{32} {I_3}^2 - 1 \leqslant 0 \tag{3.1}$$

with

$$\begin{aligned} I_1 &= \frac{1}{4}(\sigma_{22} - \sigma_{33})^2 + \sigma_{32}^2 \\ I_2 &= \sigma_{12}^2 + \sigma_{31}^2 \\ I_3 &= \sigma_{22} + \sigma_{33} \end{aligned} \tag{3.2}$$

Since the fibres behave elastically, no plastic strains are possible in fibres themselves but the matrix on the other hand can have plastic strains. This can be handled easily in micromodels, as the fibres and matrix are modelled separately with their individual material properties. However, the mesomodel is a homogenization of this microstructure and as a consequence can only take one averaged material property. Hence it is tricky to incorporate separate effects simultaneously in one stress strain relationship. Since the fibres only contribute to stresses in the fibre direction, a solution is to have separate stress tensors for the fibre stresses and matrix stresses. This can be done with an additive split of the stress tensor into the fibre stress tensor and matrix stress tensors as shown in *Eq.* 3.3 . As the matrix shows plastic behaviour, only matrix stress tensor(σ^m) will be used for evaluating the plasticity in the mesomodel.

Since the fibres only contribute to stress along the fibres, the fibres stress tensor only contains one component which is σ_{11}^f while the matrix stress tensor is fully populated with the 3D stress components. For notational simplicity, the superscript of 'f' and 'm' are written only for σ_{11} stress component among all the other stress components.

$$\sigma = \sigma^f + \sigma^m \tag{3.3}$$

The separation of stresses will hold true in an idealistic case where the fibres are perfectly straight and the matrix with voids of fibres behaves completely homogeneous. In real world this doesn't hold true as the fibres in a ply are not perfectly straight and may be intertwined with other fibres. This would cause the fibre direction stress to have components in other directions as well. It is almost impossible to determine the deviations of the fibres in an actual ply and thus compute these components in other

directions. As the deviations and overlaps are also not modeled in the microscale model, we can move forward with this additive split and avoid more complexity.

$$\sigma = \mathbf{D}^f \varepsilon + \mathbf{D}^m (\varepsilon - \varepsilon^p) \tag{3.4}$$

where

$$\mathbf{D}^f = \begin{bmatrix} f_{fib}D_{11} & 0 & 0 & 0 & 0 & 0 \\ 0 & 0 & 0 & 0 & 0 & 0 \\ 0 & 0 & 0 & 0 & 0 & 0 \\ 0 & 0 & 0 & 0 & 0 & 0 \\ 0 & 0 & 0 & 0 & 0 & 0 \\ 0 & 0 & 0 & 0 & 0 & 0 \end{bmatrix} \quad \mathbf{D}^m = \begin{bmatrix} (1-f_{fib})D_{11} & D_{12} & D_{13} & 0 & 0 & 0 \\ D_{21} & D_{22} & D_{23} & 0 & 0 & 0 \\ D_{31} & D_{32} & D_{33} & 0 & 0 & 0 \\ 0 & 0 & 0 & D_{44} & 0 & 0 \\ 0 & 0 & 0 & 0 & D_{55} & 0 \\ 0 & 0 & 0 & 0 & 0 & D_{66} \end{bmatrix} \tag{3.5}$$

The basic stress strain relationship can now be described by *Eq.* 3.4 where $\mathbf{D}^f$ contains the linear elastic stiffness of the fibres in direction '1' and $\mathbf{D}^m$ contains the elaso-plastic stiffness of the matrix in all directions as shown in *Eq.* 3.5. The population of components in the $\mathbf{D}^m$ matrix comes from assuming the matrix to be transversely isotropic with plane 2-3 being the isotropic plane. The plastic strains are only included for the matrix stresses and avoided from the fibre stress. It should be noted that when loaded in fibre direction, both the matrix and fibres carry the stress in parallel configuration. Thus both the matrix and fibres will contribute to the stiffness in direction '1' . Thus, a factor f_{fib} is introduced as percentage of stiffness contributed by only the fibre modulus in direction '1'. The value of f_{fib} is defined *Eq.* 3.6 where E_f is the elastic modulus of fibres and V_f is the fibre volume fraction in the specimen.

$$f_{fib} = \frac{E_f V_f}{D_{11}} \tag{3.6}$$

3.1.2. Modified yield function

In order to include plasticity only into the matrix via σ^m, the yield criterion needs be changed into the a function of σ^m instead of σ. To do so, new invariants are derived from the knowledge of existing invariants. The intent is to have the invariants capture the same stress states of transverse shear, in-plane shear and the biaxial stress but with the inclusion of fibre direction stress σ_{11}^m. The hydrostatic stresses are responsible for the expansion or contraction of the volume whilst the deviatoric stresses are responsible for distortions(or shearing) of the material volume. The J_2 invariant is the second invariant of the deviatoric stress tensor and serves as a good starting point. The J_2 invariant of the matrix stress tensor is given in *Eq.* 3.7 contains terms that describe the shear stresses in the matrix. Using the same I_2 as *Eq.* 3.2, we constitute the in-plane shear stresses on the matrix with $\tilde{I}_2$ (shown in *Eq.* 3.8). Since both J_2 and $\tilde{I}_2$ are invariants, the subtraction of $\tilde{I}_2$ from J_2 will also be an invariant. This invariant $\tilde{I}_1$ (shown in *Eq.* 3.9) contains terms for transverse shear and some additional shear terms. Lastly the trace of σ^m gives the hydrostatic pressure on the matrix which is given by invariant $\tilde{I}_3$ shown in *Eq.* 3.10.

$$J_2^m = \frac{1}{6}\left((\sigma_{11}^m - \sigma_{22})^2 + (\sigma_{22} - \sigma_{33})^2 + (\sigma_{33} - \sigma_{11}^m)^2\right) + \sigma_{12}^2 + \sigma_{23}^2 + \sigma_{31}^2 \tag{3.7}$$

$$\tilde{I}_2 = \sigma_{12}^2 + \sigma_{31}^2 \tag{3.8}$$

$$\tilde{I}_1 = J_2^m - \tilde{I}_2 = \frac{1}{6}\left((\sigma_{11}^m - \sigma_{22})^2 + (\sigma_{22} - \sigma_{33})^2 + (\sigma_{33} - \sigma_{11}^m)^2\right) + \sigma_{23}^2 \tag{3.9}$$

$$\tilde{I}_3 = \mathrm{tr}(\sigma^m) = \sigma_{11}^m + \sigma_{22} + \sigma_{33} \tag{3.10}$$

Having defined the new invariants, the yield function (from *Eq.* 3.1) is modified with the new invariants and is shown in *Eq.* 3.11. Each α value in the yield function represents the respective strength parameter for each stress state. Isotropic hardening is included in this model, through the α's by making them a function of the plastic internal variable. The norm of the plastic strains, called equivalent plastic strain ($\varepsilon_{\text{eq}}^{p}$) is the plastic internal variable used for this model. This is the same plastic internal variable used in Vogler et al. [28], shown in *Eq.* 3.30. Similar to the original formulation, a distinction in α_3 and α_{32} values are made for tensile and compression hydrostatic stress state (*Eq.* 3.12). This is done to take into account the fact that the matrix behaves differently in tension and compression yielding.

$$f\left(\sigma^m, \bar{\varepsilon}^p, A\right) = \alpha_1 \tilde{I}_1 + \alpha_2 \tilde{I}_2 + \alpha_3 \tilde{I}_3 + \alpha_{32} \tilde{I}_3^2 - 1 \leqslant 0 \tag{3.11}$$

with

$$\begin{aligned} &\alpha_3 = \alpha_3^t, \quad \alpha_{32} = \alpha_{32}^t \quad \text{if } I_3 > 0 \quad \text{and} \\ &\alpha_3 = \alpha_3^c, \quad \alpha_{32} = \alpha_{32}^c \quad \text{if } I_3 \leqslant 0 \end{aligned} \tag{3.12}$$

The yield function is written down using Voigt notation in a more general form as shown in *Eq.* 3.13. This form is similar to the ones present in literature and will be followed for further derivations unless mentioned otherwise. An observation can be made with $\mathbb{K}^m$ in *Eq.* 3.14 against the $\mathbb{K}$ in *Eq.* 2.16, that the first row and column are populated with terms in $\mathbb{K}^m$ as a component of fibre direction stress is included into the yield function.

$$f = \frac{1}{2}\sigma^m \cdot \mathbb{K}^m \cdot \sigma^m + \mathbb{L}^m \cdot \sigma^m - 1 \tag{3.13}$$

with

$$\mathbb{K}^m = \begin{bmatrix} 2\alpha_{32} + \frac{2}{3}\alpha_1 & 2\alpha_{32} - \frac{1}{3}\alpha_1 & 2\alpha_{32} - \frac{1}{3}\alpha_1 & 0 & 0 & 0 \\ 2\alpha_{32} - \frac{1}{3}\alpha_1 & 2\alpha_{32} + \frac{2}{3}\alpha_1 & 2\alpha_{32} - \frac{1}{3}\alpha_1 & 0 & 0 & 0 \\ 2\alpha_{32} - \frac{1}{3}\alpha_1 & 2\alpha_{32} - \frac{1}{3}\alpha_1 & 2\alpha_{32} + \frac{2}{3}\alpha_1 & 0 & 0 & 0 \\ 0 & 0 & 0 & 2\alpha_2 & 0 & 0 \\ 0 & 0 & 0 & 0 & 2\alpha_1 & 0 \\ 0 & 0 & 0 & 0 & 0 & 2\alpha_2 \end{bmatrix} \tag{3.14}$$

and

$$\mathbb{L}^m = \begin{Bmatrix} \alpha_3 & \alpha_3 & \alpha_3 & 0 & 0 & 0 \end{Bmatrix}^T \tag{3.15}$$

3.1.3. Modified Flow Rule

Having modified the yield function, the next step is to have a flow rule that compliments it. The flow rule essentially helps determine the direction of plastic flow. We know from *Eq.* 2.5 that the plastic strains are defined with a plastic multiplier $\dot{\gamma}$ and m the plastic flow direction. In theory, m is defined as the gradient to the plastic potential function in stress space *Eq.* 3.16. Thus, it is important to choose an appropriate form for the plastic potential function g for the flow rule to be compatible with the new yield function.

$$m = \frac{\partial g}{\partial \sigma} \tag{3.16}$$

Usually the flow rule has the same form as that of the yield function as can be seen from *equations* 2.12 and 2.14. Using the same ideology, the flow rule in *Eq.* 2.14 is changed by replacing the old invariants with the new invariants shown in *Eq.* 3.17. The modified flow rule presented in *Eq.* 3.17 is shown in the more general representation in *Eq.* 3.18.

$$g\left(\sigma, A\right) = \beta_1 \tilde{I}_1 + \beta_2 \tilde{I}_2 + \beta_{32} \tilde{I}_3^2 - 1 \leqslant 0 \tag{3.17}$$

or

$$g = \frac{1}{2}\sigma^m \cdot \mathbb{M}^m \cdot \sigma^m - 1 \tag{3.18}$$

where,

$$\mathbb{M}^m = \begin{bmatrix} 2\beta_{32} + \frac{2}{3}\beta_1 & 2\beta_{32} - \frac{1}{3}\beta_1 & 2\beta_{32} - \frac{1}{3}\beta_1 & 0 & 0 & 0 \\ 2\beta_{32} - \frac{1}{3}\beta_1 & 2\beta_{32} + \frac{2}{3}\beta_1 & 2\beta_{32} - \frac{1}{3}\beta_1 & 0 & 0 & 0 \\ 2\beta_{32} - \frac{1}{3}\beta_1 & 2\beta_{32} - \frac{1}{3}\beta_1 & 2\beta_{32} + \frac{2}{3}\beta_1 & 0 & 0 & 0 \\ 0 & 0 & 0 & 2\beta_2 & 0 & 0 \\ 0 & 0 & 0 & 0 & 2\beta_1 & 0 \\ 0 & 0 & 0 & 0 & 0 & 2\beta_2 \end{bmatrix} \tag{3.19}$$

The β values are defined with a constant plastic Poisson ratio(ν^p) in the original paper [28]. The following relations between the β values are given as:

$$\begin{aligned} \beta_1 &= 1 + \nu^p \\ \beta_2 &= \beta_1 = 1 + \nu^p \\ \beta_{32} &= \frac{1 - \nu^p}{4(1 + \nu^p)}\beta_1 \end{aligned} \tag{3.20}$$

where ν^p is a constant defined as:

$$\nu^p = -\frac{\varepsilon^p_{33}}{\varepsilon^p_{22}} \tag{3.21}$$

Again it is observed that the first row and column of the $\mathbb{M}^m$ is populated as opposed to $\mathbb{M}$ from *Eq.* 2.19. This is because plastic strains in '1' (or fibre) direction were left out earlier and now being considered in the new formulation. Having the terms in those places does complicate a few things though, as now it won't be correct to use a single constant ν^p to calculate the plastic strains in all directions. With the material being isotropic in 2-3 plane and plasticity ignored in '1' direction in earlier implementation, a single Poisson ratio would suffice to account for the plastic strains. However, now with the plasticity accounted for in 1 direction as well, different plastic Poisson's ratios are required as the plastic straining in 1 and 2 directions won't be similar. Because ν^p is constant and thus the entire $\mathbb{M}^m$ is constant, it would be possible to use different ν^p values for different directions for a better estimate the plastic behaviour without violating the formulations. Thus the new proposed $\mathbb{M}^m$ matrix is given in *Eq.* 3.22. The values of ν^p_{12} and ν^p_{23} are calculated from the micromodel results.

$$\mathbb{M} = \begin{bmatrix} 1 & -\nu^p_{12} & -\nu^p_{12} & 0 & 0 & 0 \\ -\nu^p_{12} & 1 & -\nu^p_{23} & 0 & 0 & 0 \\ -\nu^p_{12} & -\nu^p_{23} & 1 & 0 & 0 & 0 \\ 0 & 0 & 0 & 2\left(1 + \nu^p_{12}\right) & 0 & 0 \\ 0 & 0 & 0 & 0 & 2\left(1 + \nu^p_{23}\right) & 0 \\ 0 & 0 & 0 & 0 & 0 & 2\left(1 + \nu^p_{12}\right) \end{bmatrix} \tag{3.22}$$

3.1.4. Return Mapping

With complete expressions for the yield function and flow rules, the nonlinear relationship between the stresses and strains needs to be defined. Keeping in mind the incremental iterative procedure employed in nonlinear finite elements solvers, the relations between incremental stress and incremental strain needs to be defined. This is accomplished with a return mapping procedure where the stress increment is assumed to be fully elastic and checked for the yielding. In case the yield criterion is not satisfied, this indicates that the stress states is plastic and the stress point should exist only on the yield surface. Consequently the stress point needs to be mapped back to the yield surface. One way to do this is to compute the tangential stiffness matrix using the values at the beginning of the

load step for stress and plastic internal variable. The other way is the Euler backward method which computes the tangential stiffness matrix with the values for stress and plastic internal variable at the end load step. However, at the beginning of the load step, the final stresses are unknown and hence an iterative Newton-Raphson procedure needs to be employed to compute these values. The latter and more robust method is used for this project.

A set of equations need to be derived in order to have all the ingredients for the return mapping scheme. For simplicity in notations, the superscript m is dropped. The are presented below:

The stress at a point in the matrix can be defined as:

$$\sigma = \mathbb{D}(\varepsilon - \varepsilon_0^p - \Delta\varepsilon^p) \tag{3.23}$$

where $\mathbb{D}$ is the orthotropic elasticity tensor of the resin matrix. The ε_0^p is the initial plastic strain at the start of the load step and $\Delta\varepsilon^p$ is the change in plastic strain in that load step. The change in plastic step is defined as:

$$\Delta\varepsilon^p = \Delta\gamma \cdot \mathbf{m} \tag{3.24}$$

where, m is the direction of the plastic flow as is derived from *Eq.* 3.16 which results in:

$$\mathbf{m} = \mathbb{M}\sigma \tag{3.25}$$

Substitution gives:

$$\sigma = \mathbb{D}(\varepsilon - \varepsilon_0^p) - \mathbb{D}\Delta\gamma\mathbb{M}\sigma \tag{3.26}$$

The plastic strain at the start of the load step (ε_0^p) is known from the converged solution of previous load step. In displacement control, the total strain (ε) is also known for the load step, they are clubbed together to form the trial stress as shown in *Eq.* 3.27.

$$\sigma^{trial} = \mathbb{D}(\varepsilon - \varepsilon_0^p) \tag{3.27}$$

The stress update is then written as:

$$\sigma = \sigma^{trial} - \mathbb{D}\Delta\gamma\mathbb{M}\sigma \tag{3.28}$$

Rearranging to get σ as a function of σ^{trial}

$$\sigma = [I + \Delta\gamma\mathbb{D}\mathbb{M}]^{-1} \cdot \sigma^{tr} \equiv \mathbb{F} \cdot \sigma^{tr} \tag{3.29}$$

With this expression, σ is a function of a single unknown $\Delta\gamma$. In the yield function, the invariants are functions of σ whereas the α's are functions of the equivalent strain rate $\dot{\varepsilon}^p$. The definition of equivalent strain in Voigt notation is:

$$\dot{\varepsilon}^{\mathrm{p}}_{\mathrm{eq}} = \sqrt{\dot{\varepsilon}^{\mathrm{p}} \cdot \mathbf{J} \cdot \dot{\varepsilon}^{\mathrm{p}}} \equiv \|\dot{\varepsilon}^{\mathrm{p}}\|_{\mathrm{J}} \tag{3.30}$$

with,

$$\mathbf{J} = \mathrm{diag}\left\{\frac{1}{2}, \frac{1}{2}, \frac{1}{2}, \frac{1}{4}, \frac{1}{4}, \frac{1}{4}\right\} \tag{3.31}$$

Note that the norm $\|\dot{\varepsilon}^{\mathrm{p}}\|_{\mathrm{J}}$ is the Voigt notation equivalent of the original expression $\sqrt{\frac{1}{2}\dot{\varepsilon}^p_{ij}\dot{\varepsilon}^p_{ij}}$ found in original paper [28]. For the return mapping scheme, the finite incremental equivalent plastic strain is:

$$\Delta\varepsilon^{\mathrm{p}}_{\mathrm{eq}} = \Delta\gamma\,\|\mathbf{m}\|_{\mathrm{J}} \tag{3.32}$$

With the above expression, the equivalent plastic strains is a function of $\Delta\gamma$. The yield function is also now a function of the single unknown $\Delta\gamma$. With the value of $\Delta\gamma$ we have all the elements required to calculate the stress in the load step. The value for $\Delta\gamma$ is calculated using a local Newton-Raphson scheme which looks like:

$$\Delta\gamma^{k+1} = \Delta\gamma^{k} - \left[\frac{\partial f}{\partial \Delta\gamma}\right]^{-1} f^{k} \tag{3.33}$$

where, k is the local iteration counter for the local Newton-Raphson iternation. Keeping in mind that when the material is in a plastic state, the stresses have to lie on the yield surface, satisfying $f = 0$. Here f^k is the residual left from evaluating the yield function for the k^{th} internal variables during the return map. The term $\partial f/\partial\Delta\gamma$ is needed to interactively converge to a solution for $\Delta\gamma$. As the yield fuction f is a function of σ and $\dot{\varepsilon}^{\mathrm{p}}$ which are further functions of $\Delta\gamma$, chain rule of differentiation is applied. All the necessary derivations are presented below:

$$\frac{\partial f(\Delta\gamma)}{\partial \Delta\gamma} = \frac{\partial f\left(\sigma, \varepsilon^{\mathrm{p}}_{\mathrm{eq}}\right)}{\partial \sigma} \cdot \frac{\partial \sigma}{\partial \Delta\gamma} + \frac{\partial f\left(\sigma, \varepsilon^{\mathrm{p}}_{\mathrm{eq}}\right)}{\partial \varepsilon^{\mathrm{p}}_{\mathrm{eq}}} \frac{\partial \varepsilon^{\mathrm{p}}_{\mathrm{eq}}(\Delta\gamma)}{\partial \Delta\gamma} \tag{3.34}$$

with

$$\frac{\partial f\left(\sigma, \varepsilon^{\mathrm{p}}_{\mathrm{eq}}\right)}{\partial \sigma} = \mathbb{K} \cdot \sigma + \mathbb{L} \equiv \mathbf{n}_f \tag{3.35}$$

and

$$\frac{\partial f\left(\sigma, \varepsilon^{\mathrm{p}}_{\mathrm{eq}}\right)}{\partial \varepsilon^{\mathrm{p}}_{\mathrm{eq}}} = \frac{1}{2}\sigma \cdot \frac{\partial \mathbb{K}}{\partial \varepsilon^{\mathrm{p}}_{\mathrm{eq}}} \cdot \sigma + \frac{\partial \mathbb{L}}{\partial \varepsilon^{\mathrm{p}}_{\mathrm{eq}}} \cdot \sigma \tag{3.36}$$

Note that $\mathbb{K}$ and $\mathbb{L}$ are comprised of α's which are described by the hardening curve inputs. The hardening curve inputs are the yield strengths of the resin matrix corresponding to $\varepsilon^{\mathrm{p}}_{\mathrm{eq}}$. Thus the derivatives of $\mathbb{K}$ and $\mathbb{L}$ are directly dependent on $\varepsilon^{\mathrm{p}}_{\mathrm{eq}}$. Knowing that for a particular load step σ^{tr} is constant, differentiating *Eq.* 3.29 with respect to $\Delta\gamma$ we get:

$$[\mathbb{I} + \Delta\gamma\mathbb{D}\mathbb{M}]\frac{\partial \sigma}{\partial \Delta\gamma} + \mathbb{D}\mathbb{M}\sigma = 0 \tag{3.37}$$

or

$$\frac{\partial \sigma}{\partial \Delta\gamma} = -\mathbb{F}\mathbb{D}\mathbb{M}\sigma \tag{3.38}$$

Next the derivative of $\varepsilon^{\mathrm{p}}_{\mathrm{eq}}$ with respect to $\Delta\gamma$ is given by:

$$\frac{\partial \varepsilon^{\mathrm{p}}_{\mathrm{eq}}(\Delta\gamma)}{\partial \Delta\gamma} = \frac{\partial \varepsilon^{\mathrm{p}}_{\mathrm{eq}}(\sigma, \Delta\gamma)}{\partial \Delta\gamma} + \frac{\partial \varepsilon^{\mathrm{p}}_{\mathrm{eq}}(\sigma, \Delta\gamma)}{\partial \sigma} \cdot \frac{\partial \sigma}{\partial \Delta\gamma} \tag{3.39}$$

where,

$$\frac{\partial \varepsilon^{\mathrm{p}}_{\mathrm{eq}}(\sigma, \Delta\gamma)}{\partial \Delta\gamma} = \|\mathbf{m}\|_J \tag{3.40}$$

and

$$\frac{\partial \varepsilon^{\mathrm{p}}_{\mathrm{eq}}(\sigma, \Delta\gamma)}{\partial \sigma} = \Delta\gamma \frac{\mathrm{J} \cdot \mathbf{m}}{\|\mathbf{m}\|_{\mathrm{J}}} \cdot \mathbb{M} \tag{3.41}$$

3.1.5. Consistent Tangent Operator

The Euler backward method adopted in finding out the plastic stress for the corresponding plastic strain for a finite loading step requires a local Newton-Raphson iteration scheme. This is quite similar to the procedure employed to solve the global(structural) Newton-Raphson loop for a displacement control problem. Linearization technique applied at global level can also be applied to the local level for better convergence. For this the tangential relation for the stress rate and strain rate is derived. It start by differentiating *Eq.* 3.23

$$\sigma_n = \mathbb{D}\left(\varepsilon_n - \varepsilon^p_{n-1} - \Delta\gamma_n \mathbf{m}_n\right) \quad \Rightarrow \quad \dot{\sigma}_n = \mathbb{D}\left(\dot{\varepsilon}_n - \dot{\gamma}_n \mathbf{m}_n - \Delta\gamma \dot{\mathbf{m}}_n\right) \tag{3.42}$$

where n indicates the load step. Leaving out the subscript n, we can expand:

$$\dot{\mathbf{m}} = \mathbb{M}\dot{\sigma} \tag{3.43}$$

Substitution gives

$$\dot{\sigma}_n = \mathbb{D}\left(\dot{\varepsilon}_n - \dot{\gamma}_n \mathbf{m}_n - \Delta\gamma \mathbb{M}\dot{\sigma}\right) \tag{3.44}$$

or

$$(\mathbb{I} + \Delta\gamma \mathbb{D}\mathbb{M})\dot{\sigma} = \mathbb{D}\left(\dot{\varepsilon} - \dot{\gamma}\mathbf{m}\right) \quad \Rightarrow \quad \dot{\sigma} = \mathbb{F}\mathbb{D}\left(\dot{\varepsilon} - \dot{\gamma}\mathbf{m}\right) \tag{3.45}$$

In order to derive an expression for $\dot{\gamma}$ we make use of the consistency condition which is:

$$\dot{f} = \frac{\partial f}{\partial \sigma}\dot{\sigma} + \frac{\partial f}{\partial \varepsilon^{\mathrm{p}}_{\mathrm{eq}}}\dot{\varepsilon}^{\mathrm{p}}_{\mathrm{eq}} \tag{3.46}$$

Most of the term in the above equation are known from *Eq.* 3.35 and 3.36 except $\dot{\varepsilon}^{\mathrm{p}}_{\mathrm{eq}}$. The rate derivative of the equivalent plastic strains is:

$$\dot{\varepsilon}^{\mathrm{p}}_{\mathrm{eq}} = \frac{\partial \varepsilon^{\mathrm{p}}_{\mathrm{eq}}}{\partial \Delta\gamma}\dot{\gamma} + \frac{\partial \varepsilon^{\mathrm{p}}_{\mathrm{eq}}}{\partial \|\mathbf{m}\|_J}\|\dot{\mathbf{m}}\|_J \tag{3.47}$$

where

$$\frac{\partial \varepsilon^{\mathrm{p}}_{\mathrm{eq}}}{\partial \Delta\gamma} = \|\mathbf{m}\|_J \tag{3.48}$$

and

$$\frac{\partial \varepsilon^{\mathrm{p}}_{\mathrm{eq}}}{\|\mathbf{m}\|_J} = \Delta\gamma \tag{3.49}$$

Further, $\|\dot{\mathbf{m}}\|_J$ is derived as:

$$\|\dot{\mathbf{m}}\|_J = \frac{\partial \|\mathbf{m}\|_J}{\partial \mathbf{m}}\frac{\partial \mathbf{m}}{\partial \sigma}\dot{\sigma} = \frac{\mathrm{J}\cdot\mathbf{m}}{\|\mathbf{m}\|_{\mathrm{J}}}\cdot\mathbb{M}\dot{\sigma} \tag{3.50}$$

It is important to note while following the chain rule for differentiation in *Eq.* 3.47, at first $\|\mathbf{m}\|_J$, dependent on σ, is considered constant and then for the next term, $\Delta\gamma$ is considered constant. Substituting *equations* 3.48, 3.49 and 3.50 in *Eq.* 3.47:

$$\dot{\varepsilon}^{\mathrm{p}}_{\mathrm{eq}} = \|\mathbf{m}\|_J\,\dot{\gamma} + \Delta\gamma\frac{\mathrm{J}\cdot\mathbf{m}}{\|\mathbf{m}\|_{\mathrm{J}}}\cdot\mathbb{M}\dot{\sigma} \tag{3.51}$$

Making use of all the above derivatives and resubstituting them in the consistency condition *Eq.* 3.46

$$\dot{f} = \left(\mathbf{n}_f + \frac{\partial f\left(\sigma, \varepsilon^{\mathrm{p}}_{\mathrm{eq}}\right)}{\partial \varepsilon^{\mathrm{p}}_{\mathrm{eq}}}\Delta\gamma\frac{\mathrm{J}\cdot\mathbf{m}}{\|\mathbf{m}\|_{\mathrm{J}}}\cdot\mathbb{M}\right)\dot{\sigma} + \frac{\partial f}{\partial \varepsilon^{\mathrm{p}}_{\mathrm{eq}}}\|\mathbf{m}\|_J\,\dot{\gamma} \tag{3.52}$$

Equating $\dot{f} = 0$ to satisfy the consistency condition:

$$\dot{\gamma} = \frac{1}{\eta}\overline{\mathbf{n}}_f \dot{\sigma} \tag{3.53}$$

where

$$\overline{\mathbf{n}}_f = \mathbf{n}_f + \frac{\partial f\left(\sigma, \varepsilon_{\mathrm{eq}}^{\mathrm{p}}\right)}{\partial \varepsilon_{\mathrm{eq}}^{\mathrm{p}}} \Delta\gamma \frac{\mathrm{J}\cdot\mathbf{m}}{\|\mathbf{m}\|_{\mathrm{J}}} \cdot \mathbb{M} \tag{3.54}$$

and

$$\eta = -\frac{\partial f}{\partial \varepsilon_{\mathrm{eq}}^{\mathrm{p}}} \|\mathbf{m}\|_J \tag{3.55}$$

Now substituting the above equation in the original relationship between stress rate and strain rate (*Eq.* 3.45), we get:

$$\dot{\sigma} = \mathbb{F}\mathbb{D}\left(\dot{\varepsilon} - \frac{1}{\eta}\mathbf{m} \otimes \overline{\mathbf{n}}_f \dot{\sigma}\right) \tag{3.56}$$

Reordering gives:

$$\dot{\varepsilon} = \left[\mathbb{H}^{-1} + \frac{1}{\eta}\mathbf{m} \otimes \overline{\mathbf{n}}_f\right]\dot{\sigma} \tag{3.57}$$

here $\mathbb{H} = \mathbb{F}\mathbb{D}$. The above relation can be inverted with Sherman-Morrison formula to get the consistent tangent as:

$$\dot{\sigma} = \left[\mathbb{H} - \frac{\mathbb{H}\cdot\mathbf{m} \otimes \overline{\mathbf{n}}_f \cdot \mathbb{H}}{\eta + \overline{\mathbf{n}}_f \cdot \mathbb{H} \cdot \mathbf{m}}\right]\dot{\varepsilon} \tag{3.58}$$

3.2. Tsai Wu Yield Function

3.2.1. Context

Transverse isotropy by definition means that the properties of a material are same in one plane and different in another. It makes sense to apply this to unidirectional composites where the behaviour is different along the fibres and isotropic in directions perpendicular to the fibre direction (2-3 plane). Applying this ideology, the above constitutive relations have been formulated to account for the behaviour of fibre stresses on the matrix plasticity. However looking closely at the $\mathbb{K}^m$ matrix of the yield function in *Eq.* 3.14, we see that all yield stress parameters contributing to the axial stresses in all three directions is the same. Even the yield stress parameters that account for the interaction between axial stresses is the same. This is indicative more of isotropic behaviour and not favourable. Thus a new yield function is needed where the effects of fibre direction stresses can be accounted for individually.

A popular yield function that can incorporate the effects all stresses in three dimension on plastic behaviour of the material is the one proposed by Tsai and Wu [25]. For a three dimension special orthotropic material, the yield function reads:

$$\begin{aligned} f =& F_1\sigma_1 + F_2\sigma_2 + F_3\sigma_3 + F_{11}\sigma_{11}^2 + F_{22}\sigma_{22}^2 + F_{33}\sigma_{33}^2 + \\ & 2F_{12}\sigma_{11}\sigma_{22} + 2F_{23}\sigma_{22}\sigma_{33} + 2F_{31}\sigma_{33}\sigma_{11} + F_{44}\sigma_{44}^2 + F_{55}\sigma_{55}^2 + F_{66}\sigma_{66}^2 = 1 \end{aligned} \tag{3.59}$$

The advantage here is that the yield stress parameters (F_i's and F_{ii}'s) for each individual stress state are accounted for independently. Even the interactions between axial stresses are separately accounted for by F_{12}, F_{23} and F_{31}. This adds more flexibility to the model in tuning the effect of each stress on the nonlinear response. However, this also increases the complexity as now there are more yield stress parameters to configure the model and this might be a challenge. Since, it is desired to account for the effect of fibre direction stresses separately, we will proceed with this yield function. The additive split of the stress tensor for the homogenized mesomodel opens up the possibility for interpreting the matrix behaviour separately. Moreover, the Tsai-Wu yield criterion can be applied to the matrix independently. Thus the next subsection will present the necessary formulations for the implementation of this new yield function.

3.2.2. Yield Function

Before starting the new formulations, a few things need to be mentioned in order to be candid. First the matrix is assumed to be transversely isotropic with 2-3 plane being the plane of isotropy. Second the yield function is a function of the stress and the same plastic internal variable as previous formulations, which is the equivalent plastic strain ($\varepsilon_{\mathrm{eq}}^{\mathrm{p}}$). The yield stress parameters F_i and F_{ij} take into account isotropic hardening and are functions of the equivalent plastic strain ($\varepsilon_{\mathrm{eq}}^{\mathrm{p}}$). Lastly, an associative flow rule is assumed which defines the direction of plastic flow to be the gradient to the yield surface.

To begin the yield function is represented in a more general form as:

$$f = \frac{1}{2}\sigma^m \cdot \mathbb{P} \cdot \sigma^m + \mathbf{p} \cdot \sigma^m - 1 \tag{3.60}$$

where

$$\mathbb{P} = \begin{bmatrix} P_{11} & P_{12} & P_{12} & 0 & 0 & 0 \\ P_{12} & P_{22} & P_{23} & 0 & 0 & 0 \\ P_{12} & P_{23} & P_{22} & 0 & 0 & 0 \\ 0 & 0 & 0 & P_{44} & 0 & 0 \\ 0 & 0 & 0 & 0 & P_{55} & 0 \\ 0 & 0 & 0 & 0 & 0 & P_{44} \end{bmatrix} \tag{3.61}$$

and

$$\mathbf{p} = \begin{Bmatrix} p_1 & p_2 & p_2 & 0 & 0 & 0 \end{Bmatrix}^T \tag{3.62}$$

where in

$$P_{ii} = 2F_{ii},\ P_{12} = 2F_{12},\ p_1 = F_1,\ p_2 = F_2 \text{ and so on …} \tag{3.63}$$

3.2.3. Return Mapping

The return mapping procedure employed here is very close to the one followed previously. Nevertheless the entire set of equations required for the return mapping procedure is presented below. For simplicity in notation, the superscript m is dropped.

The stress at a point in the matrix can be defined as:

$$\sigma = \mathbb{D}(\varepsilon - \varepsilon_0^p - \Delta\varepsilon^p) \tag{3.64}$$

where $\mathbb{D}$ is the orthotropic elasticity tensor of the resin matrix. The ε_0^p is the initial plastic strain at the start of the load step and $\Delta\varepsilon^p$ is the change in plastic strain in that load step. The change in plastic step is defined as:

$$\Delta\varepsilon^p = \Delta\gamma \cdot \mathbf{n}_f \tag{3.65}$$

where, $\mathbf{n}_f$ is the gradient to the yield surface and defines the direction of plastic flow for an associative flow rule. It's expressed as:

$$\mathbf{n}_f = \frac{\partial f}{\partial \sigma} \equiv \mathbb{P}\sigma + \mathbf{p} \tag{3.66}$$

Substitution of *Eq.* 3.65 in *Eq.* 3.64 gives:

$$\sigma = \mathbb{D}(\varepsilon - \varepsilon_0^p) - \mathbb{D}\Delta\gamma\mathbf{n}_f \tag{3.67}$$

The plastic strain at the start of the load step (ε_0^p) is known from the converged solution of previous load step. Since the total strain (ε) is also known for the load step, they are clubbed together to form the trial stress as shown in *Eq.* 3.27.

The stress update is then written as:

$$\sigma = \sigma^{trial} - \Delta\gamma \mathbb{D}\mathbf{n}_f \tag{3.68}$$

Note that in this calculations it is not possible to get σ only as a function of σ^{trial}. This is due to the presence of the term $\mathbf{p}$ in the plastic flow. This does not impact the overall formulation but just changes it slightly. Moving ahead, the equivalent plastic strain is written as:

$$\dot{\varepsilon}^{\mathrm{p}}_{\mathrm{eq}} = \sqrt{\dot{\varepsilon}^{\mathrm{p}} \cdot \mathbf{J} \cdot \dot{\varepsilon}^{\mathrm{p}}} \equiv \|\dot{\varepsilon}^{\mathrm{p}}\|_{\mathrm{J}} \tag{3.69}$$

with, $\mathbf{J}$ same as in *Eq* 3.31. Using $\|\cdot\|_{\mathrm{J}}$ norm, we write the incremental equivalent plastic strains as:

$$\Delta\varepsilon^{\mathrm{p}}_{\mathrm{eq}} = \Delta\gamma \left\|\mathbf{n}_f\right\|_{\mathrm{J}} \tag{3.70}$$

For the local Newton-Raphson iteration, the term $\partial f/\partial\Delta\gamma$ is needed. It is computed as:

$$\frac{\partial f(\Delta\gamma)}{\partial\Delta\gamma} = \frac{\partial f\left(\sigma, \varepsilon^{\mathrm{p}}_{\mathrm{eq}}\right)}{\partial\sigma} \cdot \frac{\partial\sigma}{\partial\Delta\gamma} + \frac{\partial f\left(\sigma, \varepsilon^{\mathrm{p}}_{\mathrm{eq}}\right)}{\partial\varepsilon^{\mathrm{p}}_{\mathrm{eq}}} \frac{\partial\varepsilon^{\mathrm{p}}_{\mathrm{eq}}(\Delta\gamma)}{\partial\Delta\gamma} \tag{3.71}$$

with

$$\frac{\partial f\left(\sigma, \varepsilon^{\mathrm{p}}_{\mathrm{eq}}\right)}{\partial\sigma} = \mathbb{P} \cdot \sigma + \mathbf{p} \equiv \mathbf{n}_f \tag{3.72}$$

and

$$\frac{\partial f\left(\sigma, \varepsilon^{\mathrm{p}}_{\mathrm{eq}}\right)}{\partial\varepsilon^{\mathrm{p}}_{\mathrm{eq}}} = \frac{1}{2}\sigma \cdot \frac{\partial\mathbb{P}}{\partial\varepsilon^{\mathrm{p}}_{\mathrm{eq}}} \cdot \sigma + \frac{\partial\mathbf{p}}{\partial\varepsilon^{\mathrm{p}}_{\mathrm{eq}}} \cdot \sigma \tag{3.73}$$

Note that $\mathbb{P}$ and $\mathbf{p}$ are composed of the strength parameters which are described by the hardening curve inputs. The hardening curve inputs are the yield strengths of the resin matrix corresponding to $\varepsilon^{\mathrm{p}}_{\mathrm{eq}}$. Thus the derivatives of $\mathbb{P}$ and $\mathbf{p}$ are directly dependent on $\varepsilon^{\mathrm{p}}_{\mathrm{eq}}$. Knowing that for a particular load step σ^{tr} is constant, differentiating *Eq.* 3.68 with respect to $\Delta\gamma$ we get:

$$\frac{\partial\sigma}{\partial\Delta\gamma} = -\left[\mathbb{D}\mathbf{n}_f + \Delta\gamma \frac{\partial\mathbf{n}_f}{\partial\sigma} \frac{\partial\sigma}{\partial\Delta\gamma}\right] \tag{3.74}$$

where

$$\frac{\partial\mathbf{n}_f}{\partial\sigma} = \mathbb{P} \tag{3.75}$$

Thus we can rewrite *Eq.* 3.74 as:

$$\frac{\partial\sigma}{\partial\Delta\gamma}\left[\mathbb{I} + \Delta\gamma\mathbb{D}\mathbb{P}\right] = -\mathbb{D}\mathbf{n}_f \tag{3.76}$$

then

$$\frac{\partial\sigma}{\partial\Delta\gamma} = -\mathbb{A}\mathbb{D}\mathbf{n}_f \tag{3.77}$$

where $\mathbb{A} = \left[\mathbb{I} + \Delta\gamma\mathbb{D}\mathbb{P}\right]^{-1}$. Next the derivative of $\varepsilon^{\mathrm{p}}_{\mathrm{eq}}$ with respect to $\Delta\gamma$ is given by:

$$\frac{\partial\varepsilon^{\mathrm{p}}_{\mathrm{eq}}(\Delta\gamma)}{\partial\Delta\gamma} = \frac{\partial\varepsilon^{\mathrm{p}}_{\mathrm{eq}}(\sigma, \Delta\gamma)}{\partial\Delta\gamma} + \frac{\partial\varepsilon^{\mathrm{p}}_{\mathrm{eq}}(\sigma, \Delta\gamma)}{\partial\sigma} \cdot \frac{\partial\sigma}{\partial\Delta\gamma} \tag{3.78}$$

where,

$$\frac{\partial\varepsilon^{\mathrm{p}}_{\mathrm{eq}}(\sigma, \Delta\gamma)}{\partial\Delta\gamma} = \left\|\mathbf{n}_f\right\|_J \tag{3.79}$$

and

$$\frac{\partial\varepsilon^{\mathrm{p}}_{\mathrm{eq}}(\sigma, \Delta\gamma)}{\partial\sigma} = \Delta\gamma \frac{\mathrm{J} \cdot \mathbf{n}_f}{\left\|\mathbf{n}_f\right\|_{\mathrm{J}}} \cdot \mathbb{P} \tag{3.80}$$

3.2.4. Consistent Tangent Operator

In the same spirit as the previous calculations, the linearized continuum tangent operator for the local Newton-Raphson scheme is determined. The consistent tangent operator performs better in the iterative scheme employed in the finite element code and leads to faster convergence. For this the tangential relation for the stress rate and strain rate is derived. It start by differentiating *Eq.* 3.64

$$\sigma_n = \mathbb{D}\left(\varepsilon_n - \varepsilon^p_{n-1} - \Delta\gamma_n \mathbf{n}_{f_n}\right) \quad \Rightarrow \quad \dot{\sigma}_n = \mathbb{D}\left(\dot{\varepsilon}_n - \dot{\gamma}_n \mathbf{n}_{f_n} - \Delta\gamma \dot{\mathbf{n}}_{f_n}\right) \tag{3.81}$$

where n indicates the load step. Leaving out the subscript n, we can expand:

$$\dot{\mathbf{n}}_f = \mathbb{P}\dot{\sigma} + \dot{\mathbb{P}}\sigma + \dot{\mathbf{p}} \tag{3.82}$$

Care needs to be taken while deriving the above equations using chain rule. Looking at the term $\Delta\gamma\dot{\mathbf{n}}_{f_n}$ in *Eq.* 3.81, it is the rate of change of $\mathbf{n}_f$ for constant $\Delta\gamma$. Furthermore chain rule is again applied when evaluating $\dot{\mathbf{n}}_f$ which is shown in *Eq.* 3.82. Here, we are trying to find out the rate of change of $\mathbb{P}$ and $\mathbf{p}$ with respect to constant σ. Now both σ and $\Delta\gamma$ are constant and as a consequence $\dot{\mathbb{P}}$ and $\dot{\mathbf{p}}$ will be equal to zero. Thus the correct value for $\dot{\mathbf{n}}_f$ is:

$$\dot{\mathbf{n}}_f = \mathbb{P}\dot{\sigma} \tag{3.83}$$

Substitution of *Eq.* 3.83 in *Eq.* 3.81 gives

$$\dot{\sigma} = \mathbb{D}\left(\dot{\varepsilon} - \dot{\gamma}\mathbf{n}_f - \Delta\gamma\mathbb{P}\dot{\sigma}\right) \tag{3.84}$$

or

$$(\mathbb{I} + \Delta\gamma\mathbb{D}\mathbb{P})\dot{\sigma} = \mathbb{D}\left(\dot{\varepsilon} - \dot{\gamma}\mathbf{n}_f\right) \quad \Rightarrow \quad \dot{\sigma} = \mathbb{A}\mathbb{D}\left(\dot{\varepsilon} - \dot{\gamma}\mathbf{n}_f\right) \tag{3.85}$$

In order to derive an expression for $\dot{\gamma}$ we make use of the consistency condition which is:

$$\dot{f} = \frac{\partial f}{\partial \sigma}\dot{\sigma} + \frac{\partial f}{\partial \varepsilon^{\mathrm{p}}_{\mathrm{eq}}}\dot{\varepsilon}^{\mathrm{p}}_{\mathrm{eq}} \tag{3.86}$$

Most of the term in the above equation are known from *Eq.* 3.72 and 3.72 except $\dot{\varepsilon}^{\mathrm{p}}_{\mathrm{eq}}$. The rate derivative of the equivalent plastic strains is:

$$\dot{\varepsilon}^{\mathrm{p}}_{\mathrm{eq}} = \frac{\partial \varepsilon^{\mathrm{p}}_{\mathrm{eq}}}{\partial \Delta\gamma}\dot{\gamma} + \frac{\partial \varepsilon^{\mathrm{p}}_{\mathrm{eq}}}{\partial \left\|\mathbf{n}_f\right\|_J}\dot{\left\|\mathbf{n}_f\right\|}_J \tag{3.87}$$

where

$$\frac{\partial \varepsilon^{\mathrm{p}}_{\mathrm{eq}}}{\partial \Delta\gamma} = \left\|\mathbf{n}_f\right\|_J \tag{3.88}$$

and

$$\frac{\partial \varepsilon^{\mathrm{p}}_{\mathrm{eq}}}{\left\|\mathbf{n}_f\right\|_J} = \Delta\gamma \tag{3.89}$$

Further, $\dot{\left\|\mathbf{n}_f\right\|}_J$ is derived as:

$$\dot{\left\|\mathbf{n}_f\right\|}_J = \frac{\partial \left\|\mathbf{n}_f\right\|_J}{\partial \mathbf{n}_f}\frac{\partial \mathbf{n}_f}{\partial \sigma}\dot{\sigma} = \frac{\mathrm{J}\cdot\mathbf{n}_f}{\left\|\mathbf{n}_f\right\|_{\mathrm{J}}}\cdot\mathbb{P}\dot{\sigma} \tag{3.90}$$

It is important to note while following the chain rule for differentiation in *Eq.* 3.87, at first $\left\|\mathbf{n}_f\right\|_J$, dependent on σ, is considered constant and then for the next term, $\Delta\gamma$ is considered constant. Substituting *equations* 3.88, 3.89 and 3.90 in *Eq.* 3.87:

$$\dot{\varepsilon}^{\mathrm{p}}_{\mathrm{eq}} = \left\|\mathbf{n}_f\right\|_J\dot{\gamma} + \Delta\gamma\frac{\mathrm{J}\cdot\mathbf{n}_f}{\left\|\mathbf{n}_f\right\|_{\mathrm{J}}}\cdot\mathbb{P}\dot{\sigma} \tag{3.91}$$

Making use of all the above derivatives and resubstituting them in the consistency condition *Eq.* 3.86

$$\dot{f} = \left(\mathbf{n}_f + \frac{\partial f\left(\sigma, \varepsilon_{\mathrm{eq}}^{\mathrm{p}}\right)}{\partial \varepsilon_{\mathrm{eq}}^{\mathrm{p}}} \Delta\gamma \frac{\mathrm{J} \cdot \mathbf{n}_f}{\left\| \mathbf{n}_f \right\|_{\mathrm{J}}} \cdot \mathbb{P} \right) \dot{\sigma} + \frac{\partial f}{\partial \varepsilon_{\mathrm{eq}}^{\mathrm{p}}} \left\| \mathbf{n}_f \right\|_J \dot{\gamma} \tag{3.92}$$

Equating $\dot{f} = 0$ to satisfy the consistency condition:

$$\dot{\gamma} = \frac{1}{\zeta} \overline{\mathbf{n}}_f \dot{\sigma} \tag{3.93}$$

where

$$\overline{\mathbf{n}}_f = \mathbf{n}_f + \frac{\partial f\left(\sigma, \varepsilon_{\mathrm{eq}}^{\mathrm{p}}\right)}{\partial \varepsilon_{\mathrm{eq}}^{\mathrm{p}}} \Delta\gamma \frac{\mathrm{J} \cdot \mathbf{n}_f}{\left\| \mathbf{n}_f \right\|_{\mathrm{J}}} \cdot \mathbb{P} \tag{3.94}$$

and

$$\zeta = -\frac{\partial f}{\partial \varepsilon_{\mathrm{eq}}^{\mathrm{p}}} \left\| \mathbf{n}_f \right\|_J \tag{3.95}$$

Now substituting the above equation in the original relationship between stress rate and strain rate (*Eq.* 3.85), we get:

$$\dot{\sigma} = \mathbb{AD} \left(\dot{\varepsilon} - \frac{1}{\zeta} \mathbf{n}_f \otimes \overline{\mathbf{n}}_f \dot{\sigma} \right) \tag{3.96}$$

Reordering gives:

$$\dot{\varepsilon} = \left[\mathbb{B}^{-1} + \frac{1}{\zeta} \mathbf{n}_f \otimes \overline{\mathbf{n}}_f \right] \dot{\sigma} \tag{3.97}$$

here $\mathbb{B} = \mathbb{AD}$. The above relation can be inverted with Sherman-Morrison formula to get the consistent tangent as:

$$\dot{\sigma} = \left[\mathbb{B} - \frac{\mathbb{B} \cdot \mathbf{n}_f \otimes \overline{\mathbf{n}}_f \cdot \mathbb{B}}{\zeta + \overline{\mathbf{n}}_f \cdot \mathbb{B} \cdot \mathbf{n}_f} \right] \dot{\varepsilon} \tag{3.98}$$

3.3. Summary

This chapter presents two constitutive formulations based on two different yield functions. First the fibre and matrix direction stresses are separated to give more flexibility to the mesomodel. The invariants are reformulated and incorporated in a new yield function that has the same form as that proposed by Vogler et al. [28]. Using the addititve split of the stress tensor, a new yield function as proposed by Tsai and Wu [25] is tested. The complete equations necessary for the constitutive formulation are presented which include the return mapping scheme and the derivation of the consistent tangent. Next these formulations are implemented in the finite element code using the C++ JemJive[12] toolkit to model the nonlinear behaviour of a unidirectional composite material.

4

Numerical Implementation

This chapter will describe the numerical implementation of the constitutive formulations presented in the earlier chapters. It contains the material specifications used in the finite element simulations and explains the boundary conditions of the model. The derivation of the hardening curves from the micromodel is presented. These hardening curves are further used to calculate the yield stress parameters which serve as input for the mesoscale models. Lastly, the iterative procedure of the return mapping algorithm is elaborated with the help of a flow chart.

The next step after the constitutive formulations is to implement it into the finite element framework. This is done with the help of the C++ toolkit, JemJive, on representative volume element(RVE) of the fibre reinforced ply. Two types of RVEs are modelled, one is the micromodel RVE in which the fibres and matrix is modelled discretely and second the mesomodel RVE wherein the properties of fibres and matrix are represented in a homogenized manner. The micromodel RVE is modelled using the constitutive laws proposed by Melro et al. [18] with slight modifications made by Van Der Meer [27]. The mesomodel RVE is modelled using the constitutive formulations presented in *Chapter* 3. Both RVEs are modelled as plain strain and with periodic boundary conditions to represent the response in a continua.

4.1. Finite Element Model for Microscale

Composites are highly heterogeneous materials as the exact position each fibres in a ply is extremely difficult to control during manufacturing. This is because there can be microscopic deviations in fibre positions as the resin matrix sets during the curing process. Thus the cross section a ply can show different fibre positions at different material points, which makes modelling of the ply for numerical analysis quite a challenge. A common technique is to use the concept of a representative volume element(RVE), that can encapsulate the entire physical behaviour of the composite for every material point. In composite materials, a representative volume element is the smallest element size which can be used to depict, in general, the entire composite material. For microscale, this is done by taking into account an arbitrary distribution of fibres in a matrix continua as seen in *figure* 4.1.

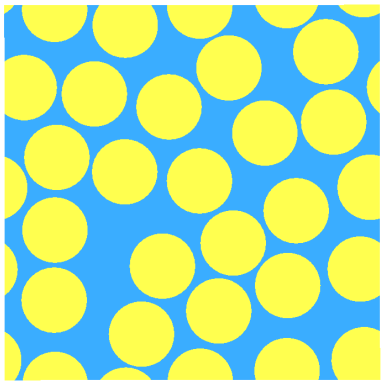

Figure 4.1: Cross sectional view of the microscale representative volume element

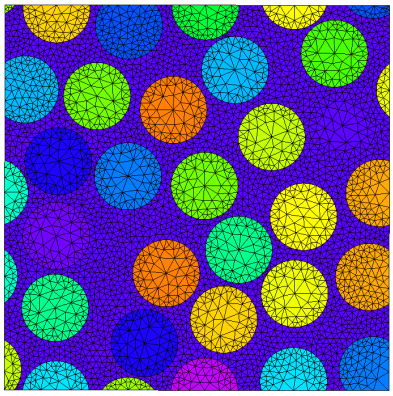

Figure 4.2: Discretized view of the microscale representative volume element

4.1.1. Representative Volume Element

The existing micromodel framework used by Van Der Meer [27] is adopted for this project. The method employed to distribute the fibres randomly in the RVE is done using the HADES simulation package. Certain geometrical parameters are set for these simulations where the diameter of the circular fibres is taken as $5\mu m$ and minimum spacing between fibres as $0.2\mu m$. A fixed number of fibres are randomly distributed in a box so as to maintain the periodicity of the element. After the study presented in [27], the RVE with 25 fibres and fibre volume fractions of 0.6 is assumed to be the representative set for generating the input and validating the mesoscale models.

The fibres are modelled as linear elastic materials and the matrix is modelled as a homogeneous isotropic material. The matrix shows isotropic hardening plasticity that is different for tension and compression. The fibres and matrix are assigned material properties as presented in *table* 4.1 for the micromodel RVE. Further this two dimensional template is discretized into three noded triangular elements using GMSH toolkit as shown in *figure* 4.2. In order to generate the three dimensional model, the two dimensional mesh is extruded out of plane to form six noded wedge elements. Next, instead

of modelling the entire ply, only a single RVE element is configured with periodic boundary conditions to reduce the computational effort.

Properties	Value
Fibres	
Young's Modulus(E)	76000 Mpa
Poisson's Ratio(ν)	0.2
Matrix	
Young's Modulus(E)	3760 Mpa
Poisson's Ratio(ν)	0.3
Plastic Poisson's Ratio(ν^p)	0.39

Table 4.1: Material properties of the fibres and matrix for the micromodel

4.1.2. Periodic Boundary Conditions

A finite element problem in statics is essentially a boundary value problem wherein the forces and supports exist on the surface of the geometry. An element inside the body is surrounded by other elements on all side, that share the same material properties. For validating constitutive laws in composites, it would be sufficient to model just a single RVE as the behaviour of the RVE should be representative for every material point in the body. In order to model a single RVE, the boundary conditions imposed by surrounding material points(or RVEs) in a continua should be taken into account properly. This is done with the help of periodic boundary conditions as shown in the *figure* 4.3.

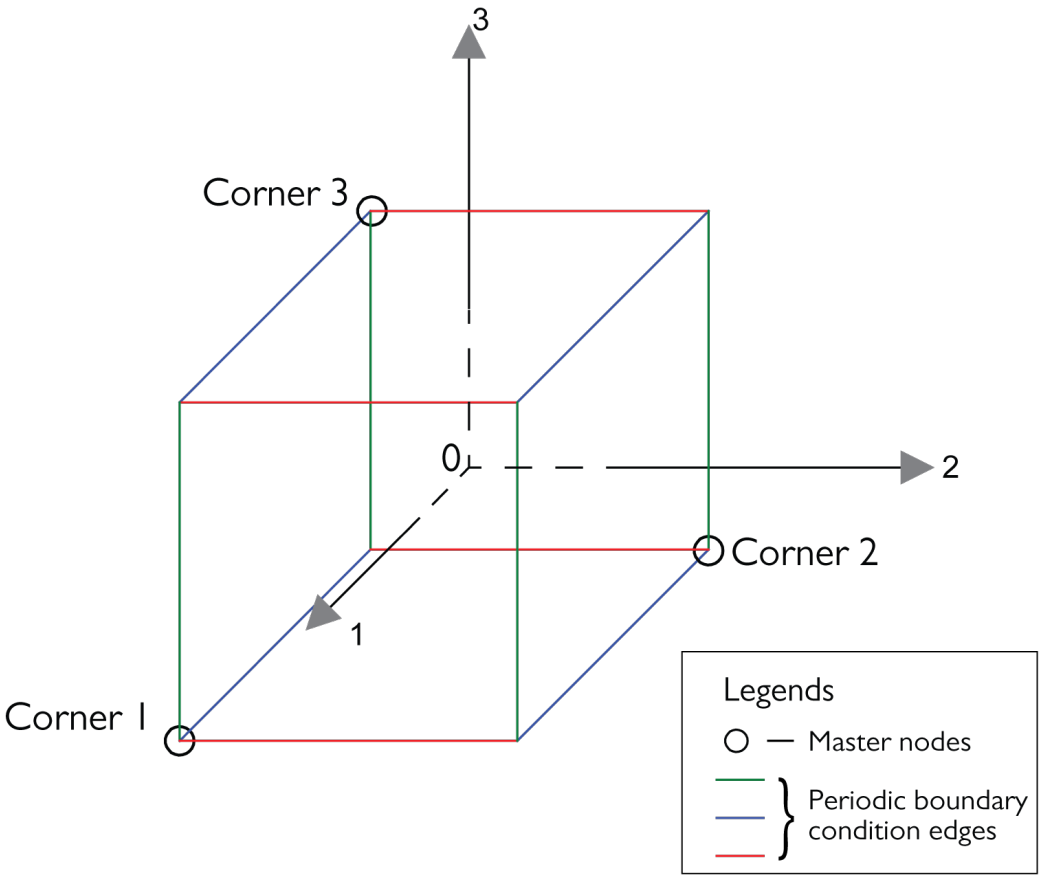

Figure 4.3: Schematic of micromodel RVE with local coordinate axes and periodic boundary conditions

To apply periodic boundary conditions, first the fibres are distributed in such a manner that the mesh

is also periodic. This means that in case a fibre is intersected by the edges of the bounding box of the matrix, the remaining area of the fibre is mirrored on the opposite edge of the box. The nodes on opposite faces of the bounding box are considered as matching nodes and their degrees of freedom are linearly constrained. According to the linear constraint, the difference between the displacements of the matching nodes is equal to the relative displacement of a master node with respect to the origin.

$$\begin{aligned}\mathbf{u}(\Delta x, y, z) &= \mathbf{u}(0, y, z) + \mathbf{u}(\Delta x, 0, 0) - \mathbf{u}(0, 0, 0)\\ \mathbf{u}(x, \Delta y, z) &= \mathbf{u}(x, 0, z) + \mathbf{u}(0, \Delta y, 0) - \mathbf{u}(0, 0, 0)\\ \mathbf{u}(x, y, \Delta z) &= \mathbf{u}(x, y, 0) + \mathbf{u}(0, 0, \Delta z) - \mathbf{u}(0, 0, 0)\end{aligned} \tag{4.1}$$

where, $\mathbf{u}(0,0,0)$ is prescribed to zero to eliminate rigid translations and $\mathbf{u}(\Delta x, 0, 0)$, $\mathbf{u}(0, \Delta y, 0)$ and $\mathbf{u}(0, 0, \Delta z)$ are three master corner nodes [27]. Displacements or forces are applied to these master nodes to obtain averaged deformations and stresses from the RVE.

4.1.3. Generation of Hardening Curves

In the scope of this project, the micromodel RVE is assumed to be representative of the actual physical behaviour of composites. Thus it is used as a substitute for extensive experimental setups to generate input data for the mesoscale RVE. The micromodel RVE is used to run simulations of basic load cases like axial tension/compression, biaxial tension/compression and pure shear along different axis. This is done in order to obtain the stress strain curves for the respective load cases from which the hardening curves for each stress state is extracted. The hardening curves serve as the required input for the calibration of the constitutive model for mesoscale.

As the material starts to exhibit plastic behaviour, a change in the stiffness of the material is observed along with plastic deformations. The point at which plastic deformations are observed, the stress at that point is known as the yield stress. Due to the nonlinear nature of the material as the strains increase, the yield stress also increases and this process is known as hardening. The stresses and strains for each load cases are monitored in the micromodel simulations in order to generate the hardening curves. Additionally, the strains on the unloaded faces are also extracted from the micromodel to obtain the Poisson's ratios. With all quantities derived, the hardening curves can be plotted with respect to the norm of the plastic strains($\varepsilon^{\mathrm{p}}_{\mathrm{eq}}$).

Equivalent Plastic Strain

The equivalent plastic strain($\varepsilon^{\mathrm{p}}_{\mathrm{eq}}$) is a scalar quantity that helps to quantify the total amount of plastic strain in the material. Hence it is also used as the plastic internal variable in the calculations of the yield function. The formula adopted for the equivalent plastic strain in this project is $\sqrt{\frac{1}{2}\varepsilon^{p}_{ij}\varepsilon^{p}_{ij}}$. Two different formulae emerge from this formula in order to calculate $\varepsilon^{\mathrm{p}}_{\mathrm{eq}}$ from the derived quantities from the micromodel simulations. For a uniaxial load test in direction '2', the two formulae look as follows:

$$\varepsilon^{\mathrm{p}}_{\mathrm{eq}} = \sqrt{\varepsilon^{p}_{11} + \varepsilon^{p}_{22} + \varepsilon^{p}_{33}} \tag{4.2}$$

and

$$\varepsilon^{\mathrm{p}}_{\mathrm{eq}} = \sqrt{\varepsilon^{p}_{22}(\nu^{p}_{12} + 1 + \nu^{p}_{23})} \tag{4.3}$$

When calculating the plastic strains for different directions, first the initial elastic stiffness is determined. Using this elastic stiffness, the elastic strains for each load step are evaluated for the corresponding stress level. Furthermore, these elastic strains are used to used to determine the respective plastic strains (refer *eq.* 2.3). Since there are no stresses in the unloaded directions of the uniaxial tests, it puzzling to distinguish the elastic and plastic strains in the unloaded directions. This is a problem only for the formula presented in *eq.* 4.2 and not for the formula in *eq.* 4.3. One possible way to determine the elastic strains for the unloaded directions is by using the elastic Poisson's ratios. With the help of that, the plastic strains in the unloaded directions can be determined. Upon evaluating the

equivalent plastic strains from both the formulae it is observed that both values do not match for the initial loads steps when the material starts to behave plastic.

An investigation revealed that there were some numerical errors when calculating the plastic strains in unloaded directions. The elastic strain in the loaded direction is multiplied by each of the elastic Poisson's ratio to obtain the elastic strains in unloaded directions respectively. For the initial plastic loading steps, these calculated elastic strains are greater than the actual total strains observed in these directions from the micromodel. This leads to incorrect estimation of plastic strains for those loading steps and hence the mismatch between the two $\varepsilon^{\mathrm{p}}_{\mathrm{eq}}$ values is observed.

On the other hand there is no need to calculate the elastic strain for the second formula of $\varepsilon^{\mathrm{p}}_{\mathrm{eq}}$ as shown in *eq* 4.3. With the help of plastic Poisson's ratios, the uniform growth of plastic strains in loaded and unloaded directions is calculated. Although the correctness of plastic Poisson's ratios is questionable as seen from Van Der Meer [27], it is the best estimate and will be used to evaluate $\varepsilon^{\mathrm{p}}_{\mathrm{eq}}$ and for defining the hardening curves.

Hardening Curves

After collecting the various stress strain inputs and calculating the equivalent plastic strains for the various load tests, the hardening curves are defined. These are the plot of yield stress with respect to the equivalent plastic strain for the different load cases. All the hardening curves obtained from the micromodel simulations are presented below.

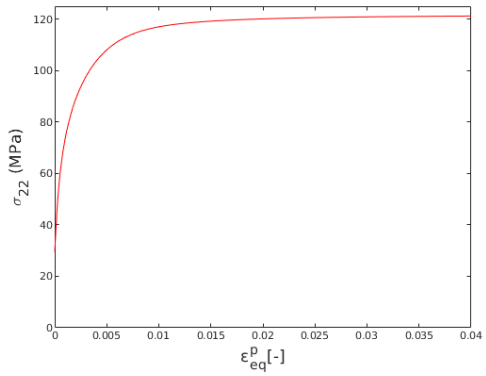

Figure 4.4: Hardening curve for uniaxial tension in transverse (or '2') direction

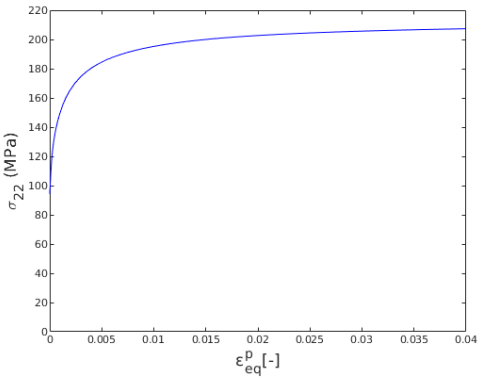

Figure 4.5: Hardening curve for uniaxial compression in transverse (or '2') direction

The hardening curves for uniaxial tension and uniaxial compression are shown in *figures* 4.4 and 4.5 respectively. It can be seen that the stress hardens till about 0.012 $\varepsilon^{\mathrm{p}}_{\mathrm{eq}}$ after which it behaves close to perfectly plastic for the uniaxial tension case. For the uniaxial compression case, the hardening is more drastic till about 0.015 after which it is quite gradual till about 0.04 $\varepsilon^{\mathrm{p}}_{\mathrm{eq}}$. Biaxial tension and biaxial compression hardening curves are shown in *figures* 4.6 and 4.7. It can be seen that the biaxial tension test shows hardening till about $0.012\varepsilon^{\mathrm{p}}_{\mathrm{eq}}$ and close to perfect plasticity for the higher $\varepsilon^{\mathrm{p}}_{\mathrm{eq}}$ values. On the other hand the biaxial compression test shows a constant hardening behaviour till about $0.016\varepsilon^{\mathrm{p}}_{\mathrm{eq}}$ after which the model fails to converge to a solution.

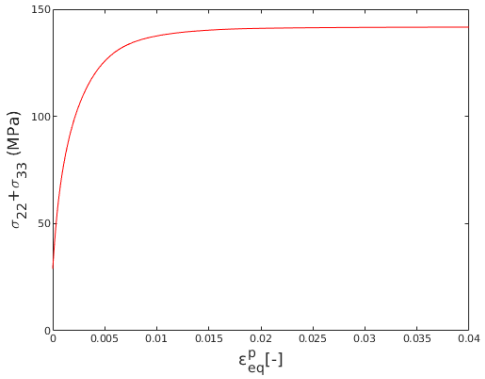

Figure 4.6: Hardening curve for biaxial tension in transverse (or '2' and '3') directions

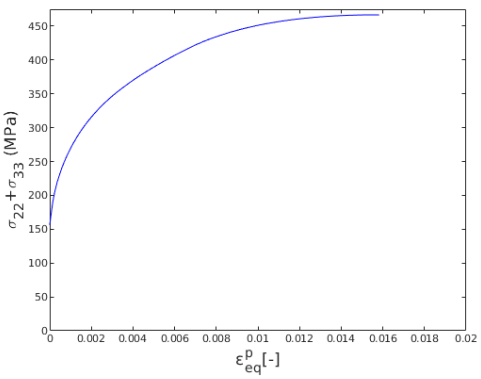

Figure 4.7: Hardening curve for biaxial compression in transverse (or '2'and '3') directions

The in-plane shear stresses and transverse shear stresses are shown in *figures* 4.8 and 4.9 respectively. For both shear stresses, significant hardening is observed till $0.01\varepsilon^p_{eq}$ after which both graphs show close to perfect plastic behaviour.

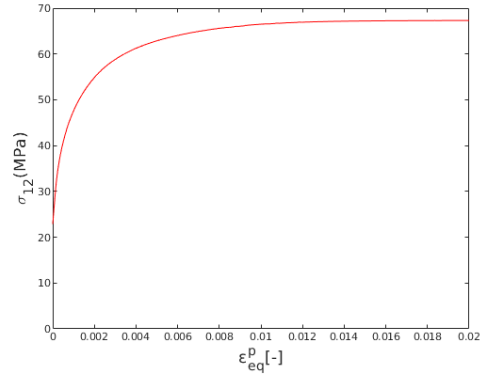

Figure 4.8: Hardening curve for in-plane shear stress

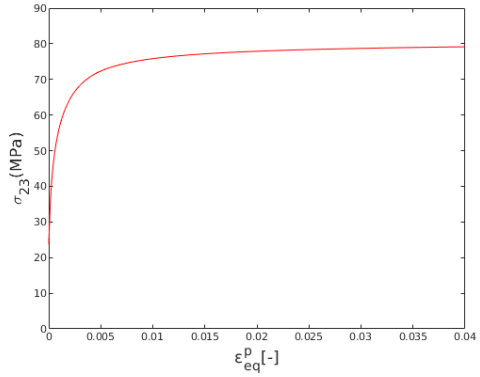

Figure 4.9: Hardening curve for transverse shear stress

Most of the hardening curves derived above can be experimentally verified. For the next set of hardening curves, that credibility might not hold, as we try to determine the yield stresses in fibre(or '1') direction but only in the matrix material. The fibres are placed along '1' direction and behave elastic, which means they will not show yielding. Thus the extraction of only the matrix stresses and not the fibre stress from a test is only possible numerically at the moment.

When the material is loaded in '1' direction, stresses are generated both in the fibres and matrix. The fibres having more strength can take higher loads/stresses than the matrix. As the loads increase, the stresses in both the fibres and the matrix increases. At some point the stresses in the matrix will reach it's yield stress and start to deform inelastically whilst at the same time the fibres will not show this inelastic behaviour. The strength of the interface between the matrix and fibres also plays an important role to determine the extent to which the matrix will deform plastically. In regions where the stresses are most concentrated, either the interface between fibres and matrix will fail or the matrix matrix might crack. This would result in redistribution of stresses and the fibres would end up taking more stresses while there might be a relaxation of stresses in the matrix. Since this process is quite complex, a simpler calculation is used to determine the stresses in the matrix.

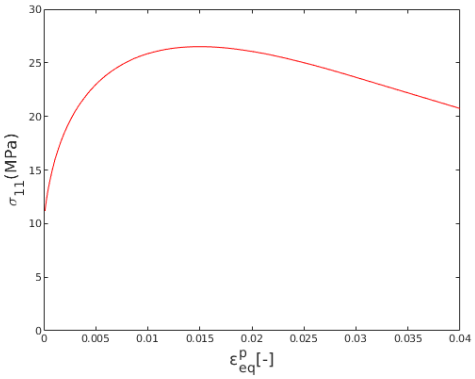

Figure 4.10: Hardening curve for the matrix stress(σ^m_{11}) in uniaxial tension under fibre (or '1') direction

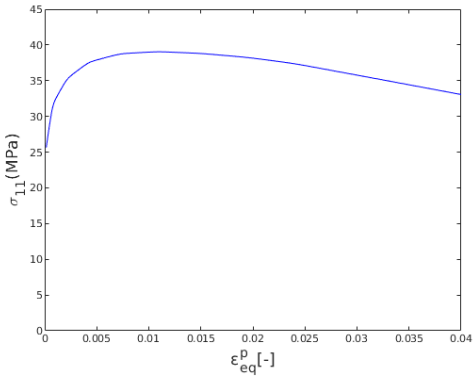

Figure 4.11: Hardening curve for the matrix stress(σ^m_{11}) in uniaxial compression under fibre (or '1') direction

At first, the initial elastic stiffness of the fibres and matrix combined is observed from the initial loads steps in the stress strain graphs. Next the elastic stiffness of only the fibres is calculated in accordance with the fibre volume fraction(value 0.6) in the RVE. As the fibres only show elastic response, the contribution of the stresses from the fibres is calculated from the total strains. On subtracting the total stresses from the fibre stresses, the stresses in the matrix is derived. These stresses are then used to plot the hardening curves presented in *figures* 4.10 and 4.11. It can be seen from those figures that initially the matrix shows a hardening response after which it quickly shows a softening response. This physically makes sense and thus will be used for further calculations.

4.2. Finite Element Model for Mesoscale

4.2.1. Representative Volume Element

Mesoscale constitutive laws can also be validated with the help of representative volume elements(RVE). The main difference between the microscale RVE and mesoscale RVE is that in microscale, the fibres and matrix are modelled discreetly with separate constitutive laws. In mesoscale, the entire element is modelled with a single constitutive law that takes into account the composite material properties by homogenization. *Figure* 4.12 helps visualize both the RVEs. Having monitored the heterogeneous response of the micromodel in various directions, necessary material constant for a homogenized mesoscale RVE can be determined.

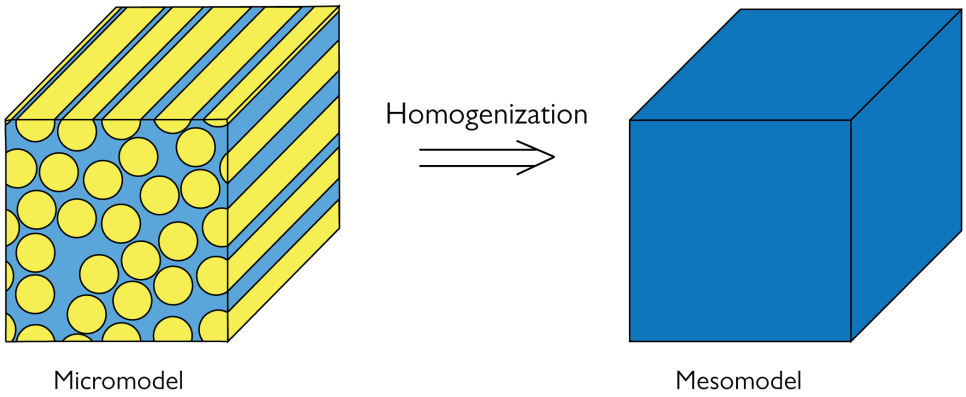

Figure 4.12: Micromodel RVE and Mesomodel RVE

Since the material properties are not the same along all directions, an orthotropic material characterization is required for the mesoscale RVE. A special case of orthotropy, which is transverse isotropy,

is used. This means that the properties are same in the 2-3 plane of local coordinate system and different in '1' direction, along which the fibres are placed. The slope of the elastic branches from the stress strain curves obtained from the simulations of the basic load cases serve as the Young's moduli. By monitoring the strains on the unloaded faces of the simulations, the Poisson's ratios for the different directions are calculated. All the orthotropic properties used for mesomodels is summed up in *table* 4.2.

Properties	Value
Young's Modulus(E_1)	45661 Mpa
Young's Modulus(E_2)	13271 Mpa
Poisson's Ratio(ν_{12})	0.23
Poisson's Ratio(ν_{23})	0.31
Plastic Poisson's Ratio(ν_{12}^p)	0.2545
Plastic Poisson's Ratio(ν_{23}^p)	0.3088
f_{fib}	0.9726

Table 4.2: Orthotropic material properties for the mesomodel

4.3. Calibration of Yield Stress Parameters

Having defined the orthotropic properties, the next step is to calibrate the unknowns in the yield functions for the mesoscale model. The unknowns in the yield functions are the α's in *eq* 4.4 and the F_i's and F_{ij}'s in *eq* 4.5. The hardening curves derived from the above exercise are used to determine these unknowns. The following paragraphs will explain how this is done for both the yield functions respectively.

$$f\left(\sigma^m, \bar{\varepsilon}^p, A\right) = \alpha_1 \tilde{I}_1 + \alpha_2 \tilde{I}_2 + \alpha_3 \tilde{I}_3 + \alpha_{32} \tilde{I}_3^2 - 1 \leqslant 0 \tag{4.4}$$

and

$$\begin{aligned} f =& F_1\sigma_1 + F_2\sigma_2 + F_3\sigma_3 + F_{11}\sigma_{11}^2 + F_{22}\sigma_{22}^2 + F_{33}\sigma_{33}^2 + \\ & 2F_{12}\sigma_{11}\sigma_{22} + 2F_{23}\sigma_{22}\sigma_{33} + 2F_{31}\sigma_{33}\sigma_{11} + F_{44}\sigma_{44}^2 + F_{55}\sigma_{55}^2 + F_{66}\sigma_{66}^2 = 1 \end{aligned} \tag{4.5}$$

4.3.1. MTIF Yield Function Calibrations

Calibrations of the yield function is done by matching the response of the mesomodel to the response of the micromodel for the same stress state. With the elastic properties mentioned in *table* 4.2, the elastic response of the mesomodel and micromodel are identical. In order for the plastic response of mesomodel to match the plastic response of the micromodel, the yield stress parameters of the yield function need to be determined. According to the theory of plasticity, the stresses in plastic regime need to satisfy the yield function. This property is used to determine the yield stress parameters. Simple load cases that were applied on the micromodel can be used to determine these parameters individually.

First, let's consider the case of transverse shear(σ_{23}), for which the corresponding yield stresses from the hardening curve can be denoted with the symbol Y_{TR}. The stress tensor for this particular stress state can be written as $\sigma^m = [0, 0, 0, 0, Y_{tr}, 0]^T$. Using this all the invariants are evaluated and inserted into the yield function and we get the following equation.

$$f\left(\sigma^m, \bar{\varepsilon}^p, A\right) = \alpha_1 Y_{TR}^2 - 1 = 0 \tag{4.6}$$

thus,

$$\alpha_1 = \frac{1}{Y_{tr}^2} \tag{4.7}$$

Similarly for in-plane shear which consider the hardening stresses as Y_{IP}, the α_2 value is evaluated as follows:

$$\alpha_2 = \frac{1}{Y_{IP}^2} \tag{4.8}$$

Next, the uniaxial tension case is considered. Care needs to be taken for this case because of the additive split of the stress tensor. When the material is loaded in transverse('2') direction, there are no stresses in other directions. In the material however, there are internal stresses present in the material in fibre('1') direction. The stresses in the fibres and the matrix are in equilibrium with each other in the fibre('1') direction. With the additive split, these stresses are accounted for separately and thus need to be accounted for in the yield stress parameter characterization. For a uniaxial tension case, the stress tensor look like $\sigma^m = \left[\sigma_{UT}^m, Y_{UT}, 0, 0, 0, 0\right]^T$. As both σ_{UT}^m and Y_{UT} appear in the $\tilde{I}_1$ and $\tilde{I}_3$, evaluating the yield function we get:

$$\alpha_1 \tilde{I}_{1,UT} + \alpha_3 \tilde{I}_{3,UT} + \alpha_{32} \tilde{I}_{3,UT}^2 - 1 = 0 \tag{4.9}$$

As there are 2 unknowns α_3 and α_{32}, and only one equation, one more equation is needed to solve for the unknowns. The biaxial tension load case is used to generate the second equation with $\sigma^m = \left[\sigma_{BT}^m, Y_{BT}, Y_{BT}, 0, 0, 0\right]^T$. From this the second equation is setup as:

$$\alpha_1 \tilde{I}_{1,BT} + \alpha_3 \tilde{I}_{3,BT} + \alpha_{32} \tilde{I}_{3,BT}^2 - 1 = 0 \tag{4.10}$$

Solving *eqns* 4.9 and 4.10 we get:

$$\alpha_3 = \frac{(\tilde{I}_{3,BT}^2 - \tilde{I}_{3,UT}^2 + \tilde{I}_{1,BT}\tilde{I}_{3,UT}^2\alpha_1 - \tilde{I}_{1,UT}\tilde{I}_{3,BT}^2\alpha_1)}{\tilde{I}_{3,UT}(\tilde{I}_{3,BT}^2 - \tilde{I}_{3,UT}\tilde{I}_{3,BT})} \tag{4.11}$$

and

$$\alpha_{32} = \frac{-(\tilde{I}_{3,BT} - \tilde{I}_{3,UT} + \tilde{I}_{1,BT}\tilde{I}_{3,UT}\alpha_1 - \tilde{I}_{1,UT}\tilde{I}_{3,BT}\alpha_1)}{\tilde{I}_{3,UT}(\tilde{I}_{3,BT}^2 - \tilde{I}_{3,UT}\tilde{I}_{3,BT})} \tag{4.12}$$

4.3.2. Tsai Wu Yield Function Calibrations

The procedure for determining the yield stress parameters for this yield function is very similar to the one presented above. Single load cases or a combination of load cases are used to determine the various parameters. First, the pure shear load case of in-plane shear is evaluated as

$$F_{44} = \frac{1}{Y_{IP}^2} \tag{4.13}$$

Due to symmetry, $F_{66} = F_{44}$ and next the pure transverse shear load case is evaluated as

$$F_{55} = \frac{1}{Y_{TR}^2} \tag{4.14}$$

For each uniaxial load case, there are two unknowns F_i and F_{ii} that need to be determined. To solve for these unknowns, the uniaxial tension and compression load cases are used to generate two sets of variables for the corresponding unknowns. Uniaxial tension and compression load case for matrix stresses(σ_{11}^m) in fibre('1') direction are presented below

$$F_1 = \left(\frac{1}{Y_{FT}} - \frac{1}{Y_{FC}}\right) \tag{4.15}$$

and

$$F_{11} = \frac{1}{Y_{FT}Y_{FC}} \tag{4.16}$$

where Y_{FT} and Y_{FC} are the yield stresses of the matrix in the fibre direction.

As mentioned above, for the uniaxial transverse tension and compression case, there is an additional component of matrix stress(σ_{11}^m) that needs to be accounted for in the evaluation of the yield function. Solving the yield function with the available yield stress values, the following equation is derived.

$$F_{11}\sigma_{11}^2 + F_{22}\sigma_{22}^2 + F_{12}\sigma_{11}\sigma_{22} + F_1\sigma_{11} + F_2\sigma_{22} - 1 = 0 \tag{4.17}$$

Note that for simplicity in notations, the superscript 'm' is dropped from the above equation. Since the material is considered to be transversely isotropic, the response in '2' direction will be identical to '3' direction. Therefore only the calculations for the unkowns in directions '2' are presented in this text.

Trial 1

Two sets of variables are known from the tension and compression load cases, however, there are three unknowns F_2,F_{22} and F_{12} which need to be solved. The term F_{12} takes into account the interaction between the axial stresses in direction '1' and '2'. So an additional biaxial load test with load applied in '1' and '2' direction is simulated using the micromodel. This simulations was carried out for the micromodel RVE that was extruded along the fibre direction for a total thickness of 0.001mm. The hardening curves derived from this simulation for both the loaded faces is presented below.

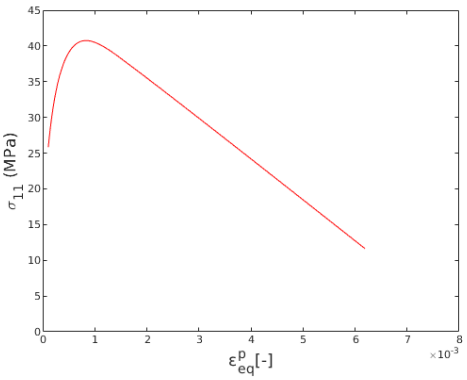

Figure 4.13: Hardening curve for the matrix stress(σ_{11}^m) under biaxial tension in fibre (or '1') direction for t = 0.001mm

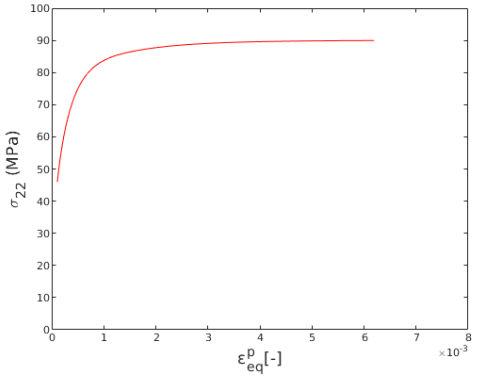

Figure 4.14: Hardening curve for the matrix stress(σ_{22}) under biaxial tension in transverse (or '2') direction for t = 0.001mm

From the above graph 4.13, it is observed that the matrix stress in fibre direction starts to soften at relatively low equivalent plastic strains. This fits well with the physical understanding that under the presence of tensile forces on the transverse face and fibre direction face, the matrix is subject to a high tensile state and will cause high stress concentrations in the matrix fibre interface. That would cause the redistribution of the stresses from the matrix to the fibres in direction '1' sooner than that observed from the uniaxial fibre direction tension case. Out of curiosity, the same biaxial tension test was carried out again, but with the micromodel RVE extruded along the fibre direction for a total thickness of 0.0286mm. Extruding to this length forms a perfect cubic three dimensional model to match the exact dimensions of the mesomodel RVE. The results from this test are presented below.

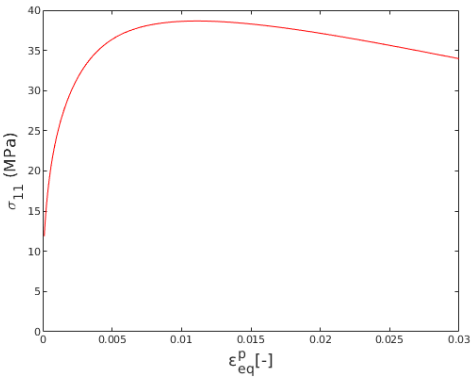

Figure 4.15: Hardening curve for the matrix stress(σ_{11}^m) under biaxial tension in fibre (or '1') direction for t = 0.0286mm

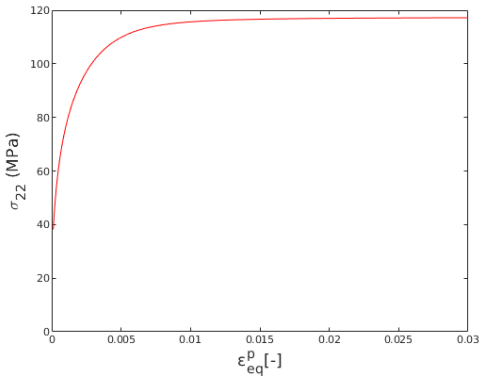

Figure 4.16: Hardening curve for the matrix stress(σ_{22}) under biaxial tension in transverse (or '2') direction for t = 0.0286mm

It can be seen from the results of this simulation that the response of both the matrix stresses is quite different from the model with thickness = 0.001mm. The softening of the matrix stresses in fibre

direction is much more gradual (refer *fig* 4.15) and the matrix stresses in transverse direction are higher than that observed from the previous simulation (refer *fig* 4.16). The cause for this might be the fact that the model with thickness = 0.0286mm has more contact area at the fibre-matrix interface to redistribute the stresses as opposed to the model with thickness = 0.001mm.

Using the two sets of knowns from the uniaxial tension and compression tests, another set is required to evaluated the unknowns F_2,F_{22} and F_{12}. These unknowns are evaluated twice, first with the third set of knowns taken from the biaxal tension test with model thickness = 0.001mm and next using the third set of knowns from the model with thickness = 0.0286mm. Thus there are two sets of F_2,F_{22} and F_{12} values available. Using either of these as input of the mesomodel, it was found that neither of these could provide for a converged solution for basic load cases. Consequently, this required for a better calibration of these three unknown parameters.

Trial 2

Instead of relying on an additional test case, it is possible to evaluate F_{12} in terms of F_{11} and F_{22} using the stability condition posed in the original paper Tsai and Wu [25]. The stability condition is stated in *equation* 4.18. The stability condition ensures that the yield surface is convex and a closed paraboloid.

$$F_{ii}F_{jj} - F_{ij}^2 \geq 0 \tag{4.18}$$

Consequently, F_{12} can be formulated as

$$F_{12} = \sqrt{F_{11}F_{22}} \tag{4.19}$$

On substituting this value in *equation* 4.17

$$F_{11}\sigma_{11}^2 + F_{22}\sigma_{22}^2 + \sqrt{F_{11}F_{22}}\sigma_{11}\sigma_{22} + F_1\sigma_{11} + F_2\sigma_{22} - 1 = 0 \tag{4.20}$$

With the presence of the square root term, this equation has two solution. Upon solving for the unknowns, it was observed that for a range of $\varepsilon_{\mathrm{eq}}^{\mathrm{p}}$ values, the solution gave imaginary roots. This makes it unfeasible to use as an input for the characterization of material properties.

Trial 3

Moving forward, numerous trials were performed with various assumptions to calibrate this yield function. Among the various trails performed, one particular solution was able to give converged solutions for basic load cases and will be discussed in this subsection whilst the other assumption are summarized in the following subsection.

An important thing to note about the yield stress parameters is that the functional form of these are not restricted. This give some freedom in choosing an appropriate form for them based on prior implementations in literature. Ideally, without the additive split of the stress tensor, the functional form of F_2 and F_{22} are very similar to the ones derived in *equations* 4.15 and 4.16 and are given below.

$$F_2 = \left(\frac{1}{Y_{UT}} - \frac{1}{Y_{UC}}\right) \tag{4.21}$$

and

$$F_{22} = \frac{1}{Y_{UT}Y_{UC}} \tag{4.22}$$

where Y_{UT} and Y_{UC} are the yield stresses of the matrix in the transverse ('2') direction.

Predetermining the functional form of all the parameters leave little freedom for the proper calibration of the model. Moreover, a balance needs to be achieved between choosing the functional forms and freedom of calibration. After numerous trials, it is found that the assuming the functional form of $F_{22} = 1/(Y_{UT}Y_{UC})$ and solving for the corresponding F_2 and F_{12} values gives converged results for basic load cases for mesomodel.

From a physical standpoint, F_{22} parameter only controls the growth of the yield stress in the transverse('2') directions. Parameter F_2 is responsible to differentiate the growth of the yield stress in tension

and compression and lastly the F_{12} takes into account the combined effect of axial stress is fibre direction on the transverse direction. As both F_2 and F_{12} aim to capture more complex non-linear effects, F_{22} on the other hand seems to be straightforward. Hence, only assuming the functional form of F_{22} and leaving the other open for calibration, helps achieve a good balance when calibrating the model. The values of the yield stress parameters obtained from this trial are the final values used in this project and for the results presented in the following chapter.

Other trials
In addition to the trials mentioned above, numerous permutations, although not some might be trivial, were considered before deciding upon the one mentioned in trial 3. Basic load cases are run with these assumption to validate the model. These trials are summarized in the table below

Trial No.	Assumptions	Observations
1	$F_2 = (1/Y_{UT} - 1/Y_{UC})$	No convergence was obtained for the pure in-plane shear load case. The transverse axial load cases showed only linear response in both tension and compression
2	$F_2 = (1/Y_{UT} - 1/Y_{UC})$ and $F_{22} = 1/(Y_{UT}Y_{UC})$	Converged solutions for pure in-plane shear load case was obtained. The transverse axial load case in tension showed largely overestimated nonlinear behaviour whilst the compression load case showed just linear response
3	$F_{12} = F_{22}$	No convergence was obtained for the pure in-plane shear load case. The transverse axial load cases showed only linear response in both tension and compression

Table 4.3: Summary of other calibration trials

4.4. Return Mapping Algorithm

The equations derived in the previous chapter are executed in a C++ code to simulate the mesomodel plastic behaviour. This section will explain how these equations are implemented and executed within the code. Also the physical understanding behind that will be explained.

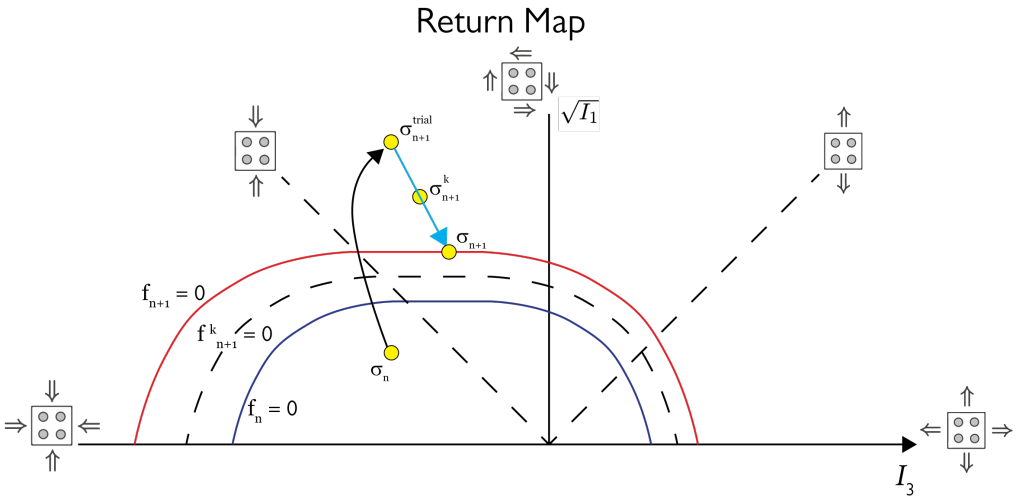

Figure 4.17: Graphical representation of the return mapping algorithm

The plastic response of the material can be understood graphically with the following *figure* 4.17. First, the yield function is marked by $f_n = 0$ and the stress point by σ_n. When the load step is incremented it is found that the stress is no more elastic and goes outside the yield surface. In order to satisfy the theory of plasticity, the stress point must lie on the yield surface. Hence the stress needs to be mapped backed to the yield surface. An additional challenge here is that isotropic hardening

is used, which expands the yield function with the increase in stress. The process of mapping back the stress point on the yield surface is done in an iterative manner and the procedure is called return mapping.

5

Results

This chapter presents the results of the finite elements simulations using the two different constitutive formulations. At first a validation of the models is performed to determine their performance. This is done by running the basic load cases that were provided as input to the model and comparing the results with the input. Next, the mesomodel is subject to a group of combined stress states for different stress ratios. The results are compared with those from the micromodel and discussed.

This chapter will present and discuss the results obtained by implementing two different constitutive models. The first constitutive law is the modified transversely isotropic invariant based formulations(MTIF) and the next one is based on Tsai and Wu's (TW) yield criterion. The results of these models are compared with the results from the micromodel(Melro) which is considered as representative for this project.

5.1. Validation of Model

The validation of the mesomodels is performed in order to check if they are able to replicate the same behaviour as micromodels for simple load cases. Since the mesomodel is calibrated using hardening curves as input, which is generated from micromodels, it makes sense to observe how the models perform for these simple load cases. As pure in-plane shear shear and pure transverse axial stress are the more realistic loading scenarios where nonlinear behaviour is pronounced, they are chosen for validation.

5.1.1. In-Plane Shear

Pure in-plane shear is obtained from the stresses on the top surface of the mesomodel RVE. The respective in plane shear strains are derived from the relative displacement of the top surface with respect to the bottom surface. The results for both MTIF and TW are shown below:

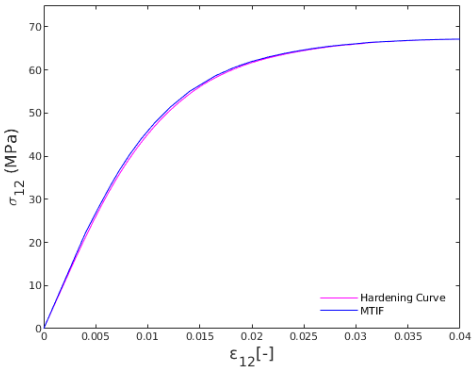

Figure 5.1: Stress strain curve for in-plane shear stresses in MTIF Mesomodel

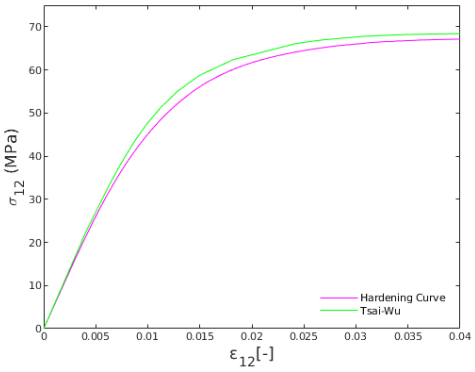

Figure 5.2: Stress strain curve for in-plane shear stresses in TW Mesomodel

It can be seen from *Fig.* 5.1 that for MTIF mesomodel, the agreement with the input hardening curve is quite good. The MTIF model is slightly more than the original curve with a mean difference of about 0.35MPa. It can be said that plastic behaviour of in pure in-plane shear is captured well by the MTIF model. On the other side, *Fig.* 5.2, the TW model is able to capture the plasticity well, but it consistently overestimates the stress by a mean difference of 1.75Mpa as compared to the prescribed hardening curve. Having conducted rigorous calibration for the TW model, this is the best fit for the loading case and has been accepted for all the further simulations.

5.1.2. Compression Transverse Axial Stress

Transverse axial strain are applied on the mesomodel RVE in the direction perpendicular to the fibres. The stresses are monitored on the surface pointing in direction '2'. The results are shown below:

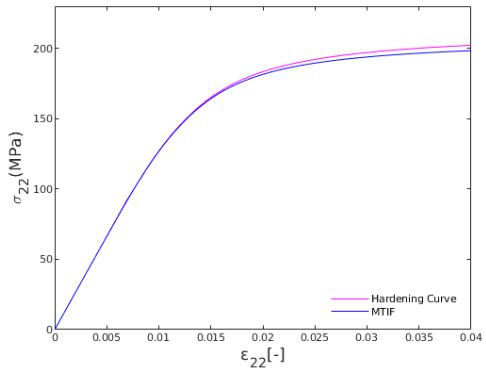

Figure 5.3: Stress strain curve for transverse axial stress(compression) in MTIF Mesomodel

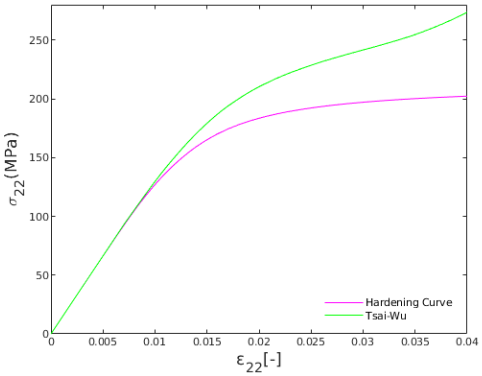

Figure 5.4: Stress strain curve for transverse axial stress(compression) in TW Mesomodel

It can be seen from *Fig.* 5.3 that for MTIF mesomodel, the plastic stresses are slightly underestimated by this model by about 2.37MPa. The reason for this can be traced to the additive split of the stress tensor which takes into account the fibre direction stresses in fibres and matrix separately. When the matrix is under transverse compression, due to Poisson's ratio there is expansion in the fibre direction however the fibres restrict this expansion. As a result the fibres provide additional confinement to the matrix. This confining effect is better predicted in the micromodel as compared to the mesomodel thus the slight shift in values are observed here.

Figure 5.4 shows the compression transverse axial response of the TW mesomodel. The results are largely overestimated with a mean difference of 35.26MPa and it even shows continued hardening as opposed to perfectly plastic behaviour observed in the micromodel for the observed strains. The calibration inaccuracy is more pronounced in this loading case than that observed in the case of pure in-plane shear. In fact the yield stress parameters(F_2,F_{22} and F_{12}) relating to the calibration of this particular stress state are the most crucial and have the most impact on the entire model.

5.1.3. Tension Transverse Axial Stress

Transverse axial strain are applied on the mesomodel RVE in the direction perpendicular to the fibres. The stresses are monitored on the surface pointing in direction 2. The results are shown below:

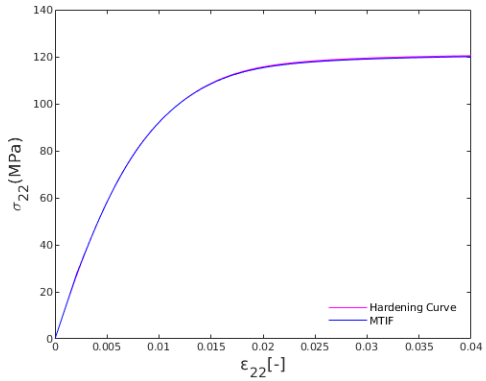

Figure 5.5: Stress strain curve for transverse axial stress(tension) in MTIF Mesomodel

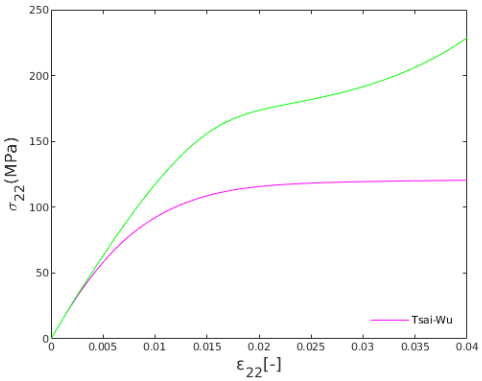

Figure 5.6: Stress strain curve for transverse axial stress(tension) in TW Mesomodel

It can be seen from *Fig.* 5.5 that for MTIF mesomodel, the plastic stresses are matching almost perfectly for the tension case as opposed to compression. The relative mean difference between the

plots is about 0.22MPa. It can be said that the interaction between the fibre direction stresses in matrix and fibres is better captured by the mesomodel in tension.

Figure 5.6 shows the tension transverse axial response of the TW mesomodel. The results are again largely overestimated by about 51 MPa on average, and it can be seen that response observed is identical to the one observed in compression. There is a small shift in the tension response than the one observed in TW model in compression. This is caused by the F_2 yield stress parameter which differentiates the response in tension and compression. Thus this parameter linearly shifts the nonlinear stresses downwards for the tension in transverse direction.

5.2. Combined stress states

Having observed the behaviour of the models for single load cases, it is interesting to find how mesomodels perform when subjected to a combination of stresses. This section will present the results of the different models when subjected to a combination of stresses expected from realistic loading scenarios.

5.2.1. Combined Axial Fibre Direction Stress and In-Plane Shear

Unidirectional laminates primarily carry loads through the fibres and in-plane shear stresses between the plies. An example of this loading is explained in *figure* 1.3 and thus will be studied with the help of the new mesomodels.

The mesomodels are subjected to multiple ratios of fibre direction stress(σ_{11}) to in-plane shear stress(σ_{12}). The results for in-plane shear are plotted as the response in fibre direction is mainly dominated by the fibres. For comparison again the Melro micromodel is used as a representative test setup for checking the results.

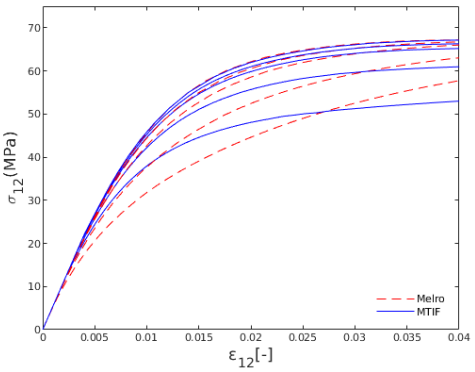

Figure 5.7: Shear stress-strain curve for combined longitudinal shear and longitudinal axial tension for ($\sigma_{11}/\sigma_{12} \in [0, 6, 11, 29, 57]$, from top to bottom) in MTIF model

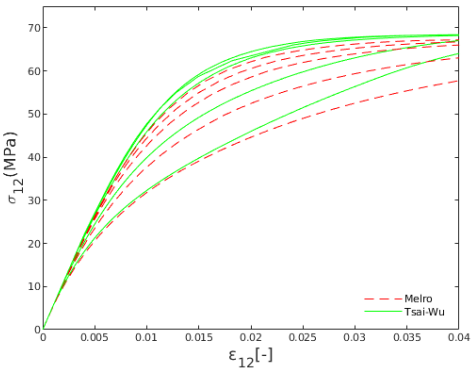

Figure 5.8: Shear stress-train curve for combined longitudinal shear and longitudinal axial tension for ($\sigma_{11}/\sigma_{12} \in [0, 6, 11, 29, 57]$, from top to bottom) in TW model

The results obtained from MTIF model are shown in *Fig.* 5.7. We can see that clearly the addition of fibre direction stresses(σ_{11}^m) has an effect on the in-plane shear stresses of the mesomodel. The trends are not good enough and the onset of plasticity for the in-plane shear stresses is not captured. For high fibre direction stresses, the matrix goes into plasticity sooner and as a result plastic in-plane shear stresses are observed at relatively low strains. This effect is not captured by the MTIF model as it uses the same yield stress parameters for all axial directions as observed from the matrix in *equation* 3.14. From hardening curves in chapter 4 it was observed that the yielding of the matrix in the fibre direction is not identical to the yielding in transverse direction. Moreover, the stress-strain plots from the MTIF model appear to be linearly scaled.

On the bright side, the TW model is able to capture the plastic behaviour of in-plane shear stresses for high fibre direction stresses as seen in *Fig.* 5.8. This can be attributed to the fact that separate yield stress parameters are used for fibre and transverse axial directions. Independently, the yield

stresses in the matrix along fibre direction softens with the increase in fibre stress while the in-plane yield stresses show hardening and tend to ideal plasticity. Thus in this combined load case, a mixed behaviour should be observed which can be predicted well with this model. The performance is better up to $\varepsilon_{12} = 0.02$ for high fibre stresses after which even the TW model start to show a more significant shift away from the micromodel results. For very low ratios of fibre stress, a subtle difference is observed in the in-plane shear with the micromodel where as the TW model results almost overlap and are slightly overestimated as observed in the validation case. This may be due to the inaccurate calibration of the transverse component parameter.

5.2.2. Combined Axial Fibre Direction Stress and Transverse Axial Direction Stress

The next most common observed stresses in a three dimensional continua is the simultaneous action of two axial stresses. Since the composite behaviour is significantly different for the fibre and transverse direction this combined stress state is explored.

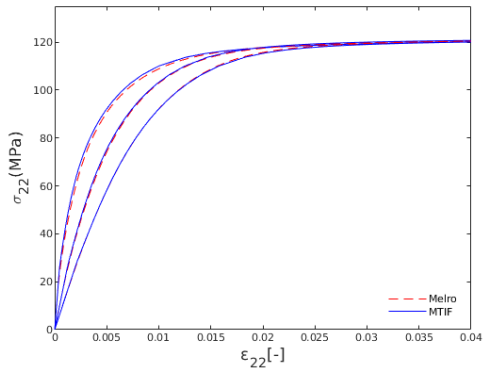

Figure 5.9: Axial stress-strain curve for combined longitudinal axial tension and transverse axial tension for ($\sigma_{11}/\sigma_{22} \in [11, 6, 0]$ from left to right) in MTIF model

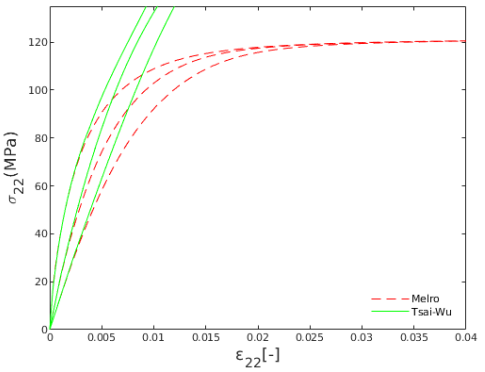

Figure 5.10: Axial stress-strain curve for combined longitudinal axial tension and transverse axial tension for ($\sigma_{11}/\sigma_{22} \in [11, 6, 0]$ from left to right) in TW model

As seen from *Fig.* 5.9 the transverse axial stress(σ_{22}) in presence of fibre direction stress(σ_{11}) is almost a perfect match for the MTIF model. This stress state gives rise to a hydrostatic expansion which is well incorporated into the yield function through the independent hardening parameters α_3 and α_{32} in tension. For low ratios, the match is perfect and co-relates well with the validation case. For the higher stress ratios, the MTIF model over predicts by a very small amount of 0.3 to 0.4 MPa on average. This also shows the capability of the model as it is able to capture the difference in behaviour for different hydrostatic loads.

Figure 5.10 shows the stress strain plot of the hydrostatic loading in the TW model. The results are well overestimated by about 150MPa on overage and the model shows ideal plastic behaviour at much higher load levels. This is because the yield stress parameters used to calibrate the transverse axial stresses is incorrect. The parameter F_{12} here is not defined well and causes this absurd plastic behaviour of the model. This parameter in particular as pointed out in the original paper [25] is very sensitive to calibration and the findings of this project verify that. Incorrect calibration could lead to the yield function not being a closed paraboloid but an open surface which can cause the instability of the solution.

5.2.3. Combined Axial Transverse Direction Stress and In-Plane Shear Stress

An interesting combination of stresses to explore would be that of the axial transverse tension and in-plane shear. Significant plastic response is observed in either of these load cases and their combined effect is investigated.

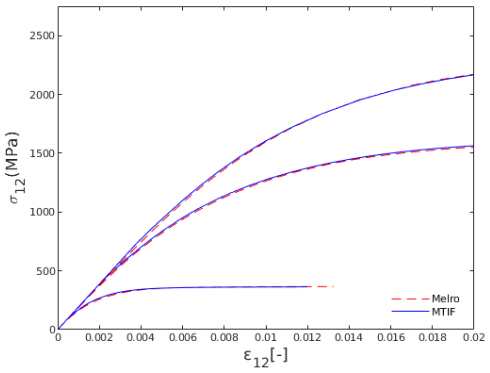

Figure 5.11: Shear stress-strain curve for combined longitudinal shear and transverse axial tension for ($\sigma_{12}/\sigma_{22} \in [11, 2, 0]$ from bottom to top) in MTIF model

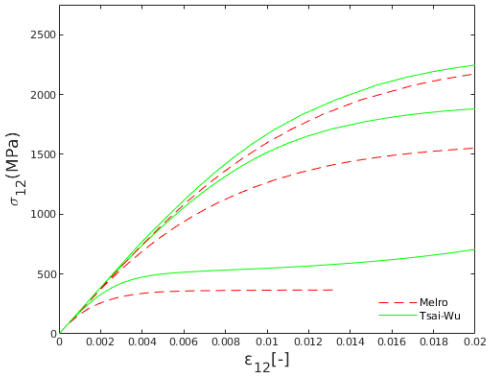

Figure 5.12: Shear stress-strain curve for combined longitudinal shear and transverse axial tension for ($\sigma_{12}/\sigma_{22} \in [11, 6, 0]$ from bottom to top) in TW model

From *figure* 5.11 it is observed that the response is highly nonlinear and show significant plastic behaviour. The MTIF model has a great match with the micromodel results with the variance in range from 0.5 to 1 MPa stress levels between the two, which is quite good for the observed magnitudes. For higher ratios of transverse shear, the response of the in-plane shear stress is significantly amplified. However, the stress levels are quite high and the matrix might fail even before reaching those stress levels in reality. Although the match and trend is good, it is difficult to make physical sense out of this test.

The results as seen from *figure* 5.12 show that the performance of the TW model is again quite poor for this combined load case. It consistently over predicts the response as compared to the micromodel and even shows some spurious hardening for higher strain levels. Again the cause for this inconsistent behaviour is due to the incorrect calibration of the TW model parameters.

5.2.4. Summary

The results of the finite elements simulations using the two different constitutive formulations are presented. The validation of the models shows that there is good agreement from the MTIF model for all three load cases where as the TW model only has acceptable results for the in-plane shear load case and poor performance in the other two. Next the results from the combined stress states are presented. The MTIF model consistently out performs the TW model for all the mixed modes cases except the longitudinal axial stress with in-plane shear test. For this particular mixed mode case the TW formulation reveals the significance of separate yield stress parameter for the fibre direction stress in the matrix.

6

Conclusions and Recommendations

Having discussed the new constitutive formulations, their implementations and results in previous chapters, this chapter discusses the concluding remarks from the study. It is followed by recommendations that could potentially help in future endeavours along this line of work.

6.1. Conclusions

Composites are heterogeneous materials that have a very complex physical behaviour. The fibres have a very high stiffness compared to the matrix and behave mostly elastic. Thus there are no plastic deformations observed along the fibres. On the other hand, the matrix is a material that exhibits nonlinear behaviour and shows plastic deformations. The fibres are impregnated with matrix and as a result, these behaviours interact with each other to form complex material response. Previously, this interaction between fibres and matrix was not taken into account explicitly by most of the yield functions defined for mesoscale models. One example of this was brought to light in the study performed by Van Der Meer [27] when comparing the yield function proposed by Vogler et al. [28] at mesoscale to the microscale model proposed by Melro et al. [18]. The study showed that the plastic response of the matrix for various levels of fibre stress was different and this was not captured by the mesoscale constitutive law. It is from this study that the research questions for this graduation project emerge. The research questions posed at the start of this project are briefly discussed below.

1. **How to incorporate the effect of fibre direction stress(σ_{11}) on the evolution of plastic in-plane shear stress(σ_{12}) within the transversely isotropic invariant based yield criterion?**

   Mesoscale models are a homogenized representation of the actual micro structure of the composite ply. Due to the inhomogeneous composition of the material, the materials are classified as orthotropic materials. Orthotropic materials have different properties along three mutually perpendicular directions. Usually a special case of orthotropy, transverse isotropy, is used to further classify unidirectional plies. This is used to define a separate material property along the direction of the fibres from the rest of the directions. This meant that the stresses in the direction of the fibres are quite high and mostly elastic while the stresses in other directions were dominated by matrix behaviour and showed non linearity. Known from the background information presented in *chapter* 2, the yield criteria are scalar functions of the stresses. Since the stresses in the fibres is very high as compared to the matrix stresses and are elastic in nature, they are not taken into account in the yield criterion formulation.

   As revealed by the study in Van Der Meer [27], the fibre direction stress needs to be incorporated to improve the accuracy of the mesoscale models. The additive split of the stress tensor into the fibre component and matrix component stress tensors is chosen for this project. This additive split enables to separately account for the elastic fibre stresses while still maintaining a component of the fibre direction stress in the matrix stress tensor. With the help of this, the transversely isotropic invariant based formulation posed by [28] is adopted. The form of the yield criterion is kept the same, but the invariants are modified in accordance with the split of the stress tensor. This is first formulation presented and implemented for the numerical analysis.

   Various tests were performed with simple load cases and combined load cases using the MTIF model. After observing the results presented in the previous chapter, the effect of fibre direction stress on the in-plane shear stresses is captured successfully. The graphs are not overlapping on each other as it did with the previous yield criterion. A shift in the in-plane shear stresses is observed. However, the behaviour only indicates a linear scaling of the graphs for various levels of fibre stress. It fails to capture the onset of matrix plasticity for the corresponding level of stress in the fibres. On the bright side, the results from most of the other combined load cases reveal that they are not affected much by this formulation changes and in some cases, the response has improved.

2. **Would an anisotropic yield criterion be able to capture the effect of the fibre direction stresses(σ_{11}) on plastic behaviour of the matrix?**

   Although the MTIF model does show promise, with it's limited yield stress parameters, it is unable to differentiate between the various plastic responses of the matrix. As observed from the yield function shown in equation 3.14, the same hardening parameters are used to quantify the plastic response of the matrix along the three mutually perpendicular directions. This is in contrast with what was observed from the hardening curves of the matrix from the micromodel simulations. The hardening curve measured in the transverse('2') direction revealed that the yield stresses in the matrix showed hardening and later stabilized to an almost ideal plastic behaviour(refer *figure* 4.4). The hardening curves for matrix stresses obtained by loading the microscale model along

the fibre('1') direction revealed a different picture(refer *figure* 4.10). The yield stress showed hardening initially, followed by a softening response for the majority of the equivalent strains values. As invariants are used to formulate the MTIF yield criterion, it becomes difficult to incorporate a different yield stress parameter for a single stress component. Thus there is a need for a better formulation.

An anisotropic yield function like the one proposed by Tsai and Wu [25], adds more flexibility to the formulation. This yield function has independent yield stress parameters which can be tuned independently according to each stress state. Because of these merits, this yield function is used as the second formulation in this project. The yield function is used along with an associated flow rule and implemented in the numerical framework. After calibration, the model was run for various stress states. With the results presented in the previous chapter, it can be said that the model shows good potential. It is able to capture good trends for the combined load case of longitudinal axial stress with longitudinal in-plane shear stress, even better than the MTIF model. However, for all other load cases, the TW model performs poorly. This is because of the difficulty faced to correctly calibrate the model.

3. **How sensitive is the anisotropic formulation to the calibration of the model?**

   With the adoption of the anisotropic yield function the constitutive formulation gains a lot of flexibility but at the same time it gets more complex. There is no proper way to determine all the yield stress parameters. Using material symmetries(transversely isotropic property), the number of independent parameters is reduced to simplify the model. As for the load cases of pure shear, the derivation of the material parameters was done in accordance with the hardening curves obtained from the micromodel simulations. Not much trouble was encountered in determining these parameters. In fact, these parameters are identical with the corresponding yield stress parameters from the MTIF model. This ensures confidence in the procedure and thus the same procedure is carried out to determine the axial yield stress parameters. It is found that F_1 and F_{11} are determined easily from the tension/compression hardening curves for that direction, however, the derivation of F_2 and F_{22} is not that simple.

   As seen from *equation* 4.17, there is an additional term F_{12} present in evaluating F_2 and F_{22}. The term F_{12} is responsible for taking into account the coupling between the stresses in the two axial directions. Ideally, this term should only be appearing if a biaxial stress states is being evaluated. But since an additive split of the stress tensor is performed at the very beginning of the formulation, the internal stress component of matrix stress in fibre direction(σ_{11}^m) is also present during pure transverse axial loading. This adds to the complexity of the problem as it is known from literature that the yield stress parameter F_{12} is very sensitive quantity.

   At first an additional test case of biaxial tension along longitudinal fibre direction and transverse axial direction was simulated. The intent of this was to generate an additional set of knonws to solve for the three unknowns. Upon further investigation it was found that the results of the biaxial tension test were subjective to the thickness of the model. To avoid subjectivity and lean towards a more general formulation, this attempt was discarded. An analytical approach that derived from the stability condition was used. Upon running simulations with this input, it was found that the model was unable to converge to a solution thus indicating that the limitation of that approach. Numerous attempts were made, each with a suitable assumption to generate a set of yield stress parameters to obtain converged solution. It is extremely difficult to correctly determine all the parameters. Among them, the assumption with $F_{22} = 1/Y_{UT}Y_{UC}$ was the best fit. After running the simulations with this assumption, for various load cases, it was observed that the parameters F_2 and F_{12} are extremely sensitive and severely impact the over behaviour of the model. This bolsters the facts mentioned in the literature about the susceptibility of the calibration input for combined stresses states.

6.2. Recommendations

It is evident that the topic addressed in the project is quite complex and certainly needs more research. With the knowledge gained from this project, a few recommendations are discussed in order to assist future endeavours along this line of work

1. **Possibility of using an additional invariant that can separately account for fibre direction stress in the MTIF yield function**

   It was observed from the MTIF formulation that the same yield stress parameters are being used for the matrix stress in transverse direction as well as fibre direction. As observed this does not hold well and thus it might interesting to look at other potential option that can help differentiate between these two behaviours without compromising the merits of the existing formulation. One possibility would be to include a separate invariant along with it's separate hardening parameter for the yielding of the matrix in the fibre direction. Some leads on this can be found in M. Vogler [16] with the I_4 invariant, however, it is important to note that the same author does not include that invariant for his future publications. It might be interesting to explore this option alongside the additive split of the stress tensor used in this project.

2. **Varying yield stress parameters with respect to fibre stress levels**

   As of now the yield stress parameters are derived from a single set of hardening curves. These hardening parameters are a function of the equivalent plastic strains. This means that the yield stress parameters consist of a single dependent value for each corresponding value of equivalent plastic strain. It can be possible to make these parameters also a function of the fibre stress levels. This can be done by generating additional hardening curves for the basic load cases like uniaxial tension/compression, biaxial tension/compression, in-plane shear and transverse shear. The level of fibre stress will be varied for these different hardening curves. As a result instead of a single input per $\varepsilon^{\mathrm{p}}_{\mathrm{eq}}$ value, now there would be a big tabular array of yield stress parameters per $\varepsilon^{\mathrm{p}}_{\mathrm{eq}}$ value. Each column would be for a different level of fibre stress. Indeed, it would be quite cumbersome to generate such a large data set to calibrate the model, and as a result slow down the simulations. This solution technique is also less robust and but is easy to implement. Hence it is worth exploring up to what extent this approach would be feasible and how much longer would the simulations run as opposed to the existing models.

3. **Use machine learning to better calibrate the strength parameters for the anisotropic formulation**

   The large data set of hardening curves as mentioned in the previous point, can be used to train a machine learning model. Not only hardening curves for single load cases but also for all combined load cases can be fed to the machine learning model. This can help improve the choice of the yield stress parameter for a particular load step for a certain values of $\varepsilon^{\mathrm{p}}_{\mathrm{eq}}$ during the simulation. A second possibility would be to try and determine the best fit for the yield stress parameter F_2 and F_{12} for the TW yield function from the large data sets. Of course the computational efforts required to generate these large data sets and also the computational efforts required by the machine learning model need to be evaluated in order to determine the overall benefits of this approach.

4. **Trial with a non-associative flow rule along with the anisotropic yield function**

   The TW constitutive formulation shows promise in it's ability to tune the various yield stress parameters for different stresses independently. Many of the calibration attempts carried out in this project were deemed unsuitable because they were not able to provide good converged solutions. Because the convexity of the yield function is a function of these yield stress parameters, it might just be that the calibrated values were appropriate. The associative flow rule used along side the yield function was maybe not able to map the stresses back to the yield surface. Thus the possibilities of a non associative flow rule along with this yield function should be explored.

Bibliography

[1] Jean-Paul Boehler and Jean-Paul Boehler. *Applications of Tensor Functions in Solid Mechanics*, volume 292. Springer, 1987.

[2] Pedro P. Camanho, Carlos G. DÃ¡vila, Silvestre T. Pinho, Lorenzo Iannucci, and Paul Robinson. Prediction of in situ strengths and matrix cracking in composites under transverse tension and in-plane shear. *Composites Part A: Applied Science and Manufacturing*, 37(2):165 – 176, 2006. ISSN 1359-835X. doi: https://doi.org/10.1016/j.compositesa.2005.04.023. URL http://www.sciencedirect.com/science/article/pii/S1359835X05002526. CompTest 2004.

[3] PP Camanho, MA Bessa, G Catalanotti, M Vogler, and R Rolfes. Modeling the inelastic deformation and fracture of polymer composites-part ii: Smeared crack model. *Mechanics of Materials*, 59:36–49, 2013.

[4] Luis P. Canal, Javier Segurado, and Javier LLorca. Failure surface of epoxy-modified fiber-reinforced composites under transverse tension and out-of-plane shear. *International Journal of Solids and Structures*, 46(11):2265 – 2274, 2009. ISSN 0020-7683. doi: https://doi.org/10.1016/j.ijsolstr.2009.01.014. URL http://www.sciencedirect.com/science/article/pii/S0020768309000341.

[5] Fu-Kuo Chang and Kuo-Yen Chang. A progressive damage model for laminated composites containing stress concentrations. *Journal of Composite Materials*, 21(9):834–855, 1987. doi: 10.1177/002199838702100904. URL https://doi.org/10.1177/002199838702100904.

[6] Prof.dr.ir. R. de Borst and Prof.dr.ir. L. J. Sluys. *Computational Methods in Non-Linear Solid Mechanics*. Delft University of Technology, Delft University of Technology, Delft, The Netherlands, 2015.

[7] Rebecca B. Dupaix and Mary C. Boyce. Constitutive modeling of the finite strain behavior of amorphous polymers in and above the glass transition. *Mechanics of Materials*, 39(1):39 – 52, 2007. ISSN 0167-6636. doi: https://doi.org/10.1016/j.mechmat.2006.02.006. URL http://www.sciencedirect.com/science/article/pii/S016766360600024X.

[8] Bassam El Said, Federica Daghia, Dmitry Ivanov, and Stephen R Hallett. An iterative multiscale modelling approach for nonlinear analysis of 3d composites. *International Journal of Solids and Structures*, 132:42–58, 2018.

[9] B Fiedler, M Hojo, S Ochiai, K Schulte, and M Ando. Failure behavior of an epoxy matrix under different kinds of static loading. *Composites Science and Technology*, 61(11):1615 – 1624, 2001. ISSN 0266-3538. doi: https://doi.org/10.1016/S0266-3538(01)00057-4. URL http://www.sciencedirect.com/science/article/pii/S0266353801000574.

[10] Elhem Ghorbel. A viscoplastic constitutive model for polymeric materials. *International Journal of Plasticity*, 24(11):2032 – 2058, 2008. ISSN 0749-6419. doi: https://doi.org/10.1016/j.ijplas.2008.01.003. URL http://www.sciencedirect.com/science/article/pii/S0749641908000119.

[11] Carlos González and Javier LLorca. Mechanical behavior of unidirectional fiber-reinforced polymers under transverse compression: Microscopic mechanisms and modeling. *Composites Science and Technology*, 67(13):2795 – 2806, 2007. ISSN 0266-3538. doi: https://doi.org/10.1016/j.compscitech.2007.02.001. URL http://www.sciencedirect.com/science/article/pii/S0266353807000711.

[12] Dynaflow Research Group. *Jive - Software Development Kit for Advanced Numerical Simulations.*, 2017. URL https://jive-manual.dynaflow.com/.

[13] Hong T. Hahn and Stephen W. Tsai. Nonlinear elastic behavior of unidirectional composite laminae. *Journal of Composite Materials*, 7(1):102–118, 1973. doi: 10.1177/002199837300700108. URL https://doi.org/10.1177/002199837300700108.

[14] I. Kaleel, M. Petrolo, E. Carrera, and A. M. Waas. Computationally efficient concurrent multiscale framework for the nonlinear analysis of composite structures. *AIAA Journal*, 57(9):4029–4041, 2019. doi: 10.2514/1.J057881. URL https://doi.org/10.2514/1.J057881.

[15] Kuo-Shih Liu and Stephen W. Tsai. A progressive quadratic failure criterion for a laminate. *Composites Science and Technology*, 58(7):1023 – 1032, 1998. ISSN 0266-3538. doi: https://doi.org/10.1016/S0266-3538(96)00141-8. URL http://www.sciencedirect.com/science/article/pii/S0266353896001418.

[16] R. Rolfes M. Vogler, G. Ernst. Invariant based transversely-isotropic material and failure model for fiber-reinforced polymers. *Computers, Materials & Continua*, 16(1):25–50, 2010. ISSN 1546-2226. doi: 10.3970/cmc.2010.016.025.

[17] P. Maimí, P.P. Camanho, J.A. Mayugo, and A. Turon. Matrix cracking and delamination in laminated composites. part i: Ply constitutive law, first ply failure and onset of delamination. *Mechanics of Materials*, 43(4):169 – 185, 2011. ISSN 0167-6636. doi: https://doi.org/10.1016/j.mechmat.2010.12.003. URL http://www.sciencedirect.com/science/article/pii/S0167663610001663.

[18] AR Melro, PP Camanho, FM Andrade Pires, and ST Pinho. Micromechanical analysis of polymer composites reinforced by unidirectional fibres: Part i–constitutive modelling. *International Journal of Solids and Structures*, 50(11-12):1897–1905, 2013.

[19] AR Melro, PP Camanho, FM Andrade Pires, and ST Pinho. Micromechanical analysis of polymer composites reinforced by unidirectional fibres: Part ii–micromechanical analyses. *International Journal of Solids and Structures*, 50(11-12):1906–1915, 2013.

[20] Yongli Mi and Sixun Zheng. A new study of glass transition of polymers by high pressure dsc. *Polymer*, 39(16):3709 – 3712, 1998. ISSN 0032-3861. doi: https://doi.org/10.1016/S0032-3861(97)10357-3. URL http://www.sciencedirect.com/science/article/pii/S0032386197103573.

[21] Robin Olsson. A survey of test methods for multiaxial and out-of-plane strength of composite laminates. *Composites Science and Technology*, 71(6):773 – 783, 2011. ISSN 0266-3538. doi: https://doi.org/10.1016/j.compscitech.2011.01.022. URL http://www.sciencedirect.com/science/article/pii/S0266353811000509.

[22] KD Pae and KY Rhee. Effects of hydrostatic pressure on the compressive behavior of thick laminated 45° and 90° unidirectional graphite-fiber/epoxy-matrix composites. *Composites science and technology*, 53(3):281–287, 1995.

[23] Juan C Simo and Thomas JR Hughes. *Computational Inelasticity*, volume 7. Springer Science & Business Media, 2006.

[24] AJM Spencer. Plasticity theory for fibre-reinforced composites. *Journal of engineering mathematics*, 26(1):107–118, 1992.

[25] Stephen W Tsai and Edward M Wu. A general theory of strength for anisotropic materials. *Journal of composite materials*, 5(1):58–80, 1971.

[26] FP Van Der Meer and LJ Sluys. Continuum models for the analysis of progressive failure in composite laminates. *Journal of Composite Materials*, 43(20):2131–2156, 2009.

[27] Frans P Van Der Meer. Micromechanical validation of a mesomodel for plasticity in composites. *European Journal of Mechanics-A/Solids*, 60:58–69, 2016.

[28] M Vogler, R Rolfes, and PP Camanho. Modeling the inelastic deformation and fracture of polymer composites-part i: plasticity model. *Mechanics of Materials*, 59:50–64, 2013.

[29] Junjie Ye, Yuanying Qiu, Zhi Zhai, Xuefeng Chen, and Yuchen Fan. Investigation of the effect of microstructural parameters on the initial yield surface of non-isothermal composites. *Science and Engineering of Composite Materials*, 22(6):613 – 621, 2015. doi: https://doi.org/10.1515/secm-2013-0244. URL https://www.degruyter.com/view/journals/secm/22/6/article-p613.xml.